Locomotion-dependent auditory gating to the parietal cortex guides multisensory decisions

Ilsong Choi[1], Seung-Hee Lee[1,2*]

[1]Center for Synaptic Brain Dysfunctions, IBS, Daejeon, 34141, Republic of Korea

[2]Department of Biological Sciences, KAIST, Daejeon, 34141, Republic of Korea

*Correspondence and requests for materials should be addressed to S.-H.L. (e-mail: shlee1@kaist.ac.kr).

Abstract

Decision-making in mammals fundamentally relies on integrating multiple sensory inputs, with conflicting information resolved flexibly based on a dominant sensory modality. However, the neural mechanisms underlying state-dependent changes in sensory dominance remain poorly understood. Our study demonstrates that locomotion in mice shifts auditory-dominant decisions toward visual dominance during audiovisual conflicts. Using circuit-specific calcium imaging and optogenetic manipulations, we found that weakened visual representation in the posterior parietal cortex (PPC) leads to auditory-dominant decisions in stationary mice. Prolonged locomotion, however, promotes visual dominance by inhibiting auditory cortical neurons projecting to the PPC (AC_{PPC}). This shift is mediated by secondary motor cortical neurons projecting to the auditory cortex ($M2_{AC}$), which specifically inhibit AC_{PPC} neurons without affecting auditory cortical projections to the striatum (AC_{STR}). Our findings reveal the neural circuit mechanisms underlying auditory gating to the association cortex depending on locomotion states, providing insights into the state-dependent changes in sensory dominance during multisensory decision-making.

Introduction

Multisensory integration in the brain, which combines neural information from different sensory modalities, is essential for goal-directed perceptual decisions in an ever-changing environment[1]. Animals can make faster[2,3] and more accurate[4,5] perceptual decisions when they integrate congruent (coherent) multisensory stimuli. On the other hand, animals frequently prioritize one modality over the other in response to conflicting multisensory stimuli and show sensory dominance in their perceptual decisions[6-13]. For instance, when head-fixed mice faced conflicting audiovisual cues (one instructed 'Go' responses while the other instructed 'No-go' responses), they often made decisions following auditory cues[12,13]. This sensory dominance in multisensory decisions cannot be fully explained by a simple additive integration of individual stimuli as explained by a classic Bayesian model[14-16]. Rather, it requires under-weighting one modality more than the other before the integration[10,11,17], potentially via cross-modal inhibition[12,18,19]. Interestingly, the prepotent modality in multisensory decisions not only varies individually but also switches flexibly from trial to trial[10,11,20,21]. Neural underpinnings of such changes in sensory dominance, however, remain largely unexplored.

Perceptual decision-making occurs with sensory representation associated with motor actions across cortical areas[22,23]. The sensory representation is not stable and fluctuates depending on the behavioral states of the animals[24,25]. One key factor affecting the cortical representation of sensory stimuli is the locomotion. Locomotion increases arousal, which amplifies visual gain in the visual cortex (VC)[26-34] but suppresses auditory representations in the auditory cortex (AC)[35,36]. Furthermore, locomotion generates corollary discharge signals copied from motor commands, which also suppress auditory responses in the AC[37,38]. As a result of these representational changes, mice showed better detection of mild visual cues[27] and reduced detection of weak auditory cues[35,39]. Despite this, animals still can identify salient

auditory cues well and perform auditory-dependent perceptual tasks without disruption even during locomotion[40,41]. These reports suggest that, even during locomotion, animals retain salient auditory information in the brain, enabling them to make appropriate auditory decisions. In a multisensory environment containing both visual and auditory stimuli, it is more challenging to determine how locomotion influences the multisensory representation and decision-making processes. Compared to head-fixed mice, freely roaming mice exhibited no differences in unisensory decisions but only shifted prepotent modality from audition to vision during multisensory decisions[13]. However, it is unclear how locomotion modulates neural circuits representing multisensory stimuli in the brain to alter behavioral decisions in mice.

One of the key brain areas that mediate perceptual decision-making is the posterior parietal cortex (PPC)[42-44]. The PPC encodes various task-relevant activities during visual decision-making tasks. For example, the PPC conveys visual information[45-48], accumulating sensory evidence[49,50], history of the task variables[47,51], animal's choices[45,47,52-54], and body movements[55]. Furthermore, inactivation of the PPC resulted in a substantial decline in an animal's ability to make visual decisions[45,53,56]. Similar to the visual activities, the PPC also showed task-relevant activities during auditory decision-making tasks[47,56-59]. Its inactivation, however, did not impair perceptual decisions based on simple auditory cues, such as feature detection or discrimination in well-trained animals[48,56,60]. Instead, PPC activity was required for more complex auditory-dependent decision-making, which involves higher levels of cognitive processing[58,61,62]. The PPC receives converging inputs from visual, auditory, and somatosensory cortices[63-65] and responds to multisensory stimuli in humans[66], primates[19,67] and rodents[68,69]. However, its role in multisensory decisions is still unclear. PPC inactivation altered multisensory decisions under audiovisual conflicts[12] (but see also[16]), but it did not affect multisensory decisions in coherent conditions[16,56]. These reports suggest that the PPC in

75 multisensory decisions may depend on the task paradigms or multisensory contexts that the
76 animal encounters.

77 To understand how the PPC is involved in multisensory decisions in animals making
78 perceptual decisions across auditory, visual, and congruent or incongruent audiovisual stimuli,
79 at different behavioral states, we used *in vivo* calcium imaging and optogenetic manipulation
80 techniques in mice performing an audiovisual discrimination task on the treadmill. We
81 discovered that the dominant modality can be switched from audition to vision during
82 locomotion. The PPC neurons discriminated visual inputs better than auditory inputs, and the
83 visual representation was suppressed when animals made auditory-dominant decisions in
84 audiovisual conflicts. During locomotion, the AC output to the PPC (AC_{PPC}) was selectively
85 suppressed, while the AC output to the striatum (AC_{STR}) was maintained. This circuit-specific
86 modulation preserved the visual representation in the PPC and allowed animals to make
87 visually dominant multisensory decisions when animals confronted conflicting audiovisual
88 stimuli during locomotion. The locomotion-induced suppression of AC_{PPC} neurons was
89 mediated by top-down inputs from the secondary motor cortex (M2) to the AC. Our data
90 demonstrate a neural mechanism of switching sensory dominance in the face of cross-modal
91 conflicts, which require gating in the auditory-to-parietal circuit according to the animal's
92 behavioral states.

Results

Locomotion enhances visually dominant decisions in mice under audiovisual conflicts

To examine state-dependent multisensory decisions in mice, we trained head-fixed mice to discriminate auditory and visual stimuli and make Go/No-go decisions on a non-motorized treadmill (Fig. 1a,b; 10 kHz vs. 5 kHz pure-tones: auditory Go (A_G) vs. auditory No-go (A_{NG}); vertically vs. horizontally drifting gratings: visual Go (V_G) vs. visual No-go (V_{NG})). After mice became experts in discriminating both auditory and visual stimuli at similar correct rates in the stationary (S) state (Fig. 1c), we compared their performance in the moving (M) state (Fig. 1d). During the test, either congruent (A_GV_G or $A_{NG}V_{NG}$) or incongruent (A_GV_{NG} or $A_{NG}V_G$) audiovisual stimuli were randomly presented in a certain ratio (25% or 40%) of trials to examine their licking decisions in this multisensory context (Fig. 1e). During incongruent trials, mice made either auditory-dominant or visual-dominant decisions (Fig. 1e; Methods). Head-fixed mice showed better performance of discriminating congruent audiovisual stimuli compared to auditory- or visual-only stimuli in stationary conditions (Fig. 1f and Supplementary Fig. 1a). In moving sessions, the same mice discriminated the unisensory (auditory or visual) stimuli better, often hit the maximum performances, and therefore showed no further improvement in congruent trials (Fig. 1f and Supplementary Fig. 1a). As reported previously[12], stationary mice showed auditory-dominant decisions in response to the incongruent audiovisual stimuli (Fig. 1g and Supplementary Fig. 1b; 80.7% of incongruent trials). Interestingly, the moving mice made considerably fewer auditory-dominant decisions (Fig. 1g and Supplementary Fig. 1b; 45.6% of incongruent trials). This enhanced visual dominance (decreased auditory dominance) was not significantly correlated with enhanced visual discrimination (Supplementary Fig. 1c), suggesting that improvements in visual discrimination do not solely account for locomotion-dependent changes in the dominant sensory modality during multisensory decisions.

We further examined the effects of different conditions of locomotion on switching auditory dominance to visual dominance. First, we examined the effect of locomotion duration, as it has been shown that the locomotion-induced changes in cortical states depend on its duration[36,38,70,71]. We compared mice's decisions in incongruent trials when the stimuli were presented right after locomotion (start-moving, SM) with those when stimuli were presented after prolonged (> 3s) locomotion (keep-moving, KM). Interestingly, mice showed stronger visual dominance in the keep-moving trials than in the start-moving trials (Fig. 1h and Supplementary Fig. 1b). Once they kept moving at a certain speed (> 3cm/s), the pre-stimulus speed did not further affect their decisions in incongruent trials (Supplementary Fig. 1d). These data indicate that the duration, not the speed, of locomotion is important for switching the dominant modality from audition to vision in mice making decisions under audiovisual conflicts. The unisensory trial types and outcomes of previous trials did not affect the mice's decision in incongruent trials with or without locomotion (Supplementary Fig. 1e). The level of arousal measured by pupil size was also unrelated to the effect of locomotion on changes in dominant decisions (Supplementary Fig. 1f,g). We also examined whether licking behavior was affected by locomotion (Supplementary Fig. 1h-k). Lick reaction times and post-stimulus lick rates in hit trials were not altered by locomotion (Supplementary Fig. 1i,j), but spontaneous licking before stimulus onset was significantly reduced in the moving state (Supplementary Fig. 1k). However, reduced pre-stimulus licking was not different between auditory-dominant and visual-dominant trials, indicating that pre-stimulus licking did not directly influence the licking decision in multisensory trials (Supplementary Fig. 1k). Therefore, the duration of locomotion prior to stimulus onset, compared to any other internal factors, is the most critical factor determining which modality becomes dominant.

PPC perturbation enhances auditory dominance and impairs visual discrimination

143 In our previous study, we found that the feed-forward auditory-to-visual inhibitory
144 circuit in the PPC is critical for mediating auditory dominance in mice performing an
145 audiovisual detection (not discrimination) task in a head-fixed, stationary state[12]. In the present
146 study, we introduced a behavioral paradigm that measured auditory, visual, and audiovisual
147 discrimination in the same mouse. Similarly, we observed auditory dominance during
148 audiovisual conflicts in stationary mice (Fig. 1g,h). Building on these findings, we next
149 examined whether the PPC is required for behavioral decisions during this discrimination task
150 in a stationary state. First, we bilaterally injected muscimol, a $GABA_A$ receptor agonist, to
151 suppress PPC activity in task-performing mice (Fig. 2a). PPC inactivation resulted in a severe
152 impairment of visual discrimination but did not affect auditory discrimination in stationary
153 mice (Fig. 2b). This imbalance led to more pronounced auditory-dominant decisions during
154 incongruent trials (Fig. 2b) and reduced multisensory enhancement during congruent trials (Fig.
155 2c).

156 Next, we locally inactivated the PPC in task-performing stationary mice by
157 optogenetically activating parvalbumin-expressing (PV^+) neurons in the region (Fig. 2d). Mild
158 activation of PV^+ neurons with a 1 mW laser caused mice to make more auditory-dominant
159 decisions during incongruent trials, while visual discrimination and congruent multisensory
160 enhancement remained intact (Fig. 2e,f). Stronger inactivation of the PPC, achieved using a
161 higher laser power (5 mW), resulted in impairments in visual discrimination and multisensory
162 enhancement similar to those observed under muscimol inactivation conditions (Fig. 2g-j).
163 Interestingly, while robust PPC inactivation impaired visual discrimination, mild activation of
164 PV^+ inhibitory neurons enhanced auditory dominance without affecting visual discrimination
165 (Fig. 2e,f,i,j), consistent with our previous findings[12]. Collectively, these results demonstrate
166 that PPC inactivation strengthens auditory dominance in multisensory incongruent trials and
167 highlight that PPC activity is essential for visual discrimination but not auditory discrimination.

168

169 **Locomotion reduces auditory representation in the PPC**

170 As the PPC activity is important for mice to make perceptual decisions by integrating
171 auditory and visual inputs[12], we next examined how the PPC excitatory neurons represent task-
172 relevant sensory information in mice performing the audiovisual discrimination task by *in vivo*
173 calcium imaging using a miniature microscope through a prism-combined gradient reflective
174 index (GRIN) lens (Fig. 3a). We first classified neuronal types based on their responses to
175 different sensory stimuli in unisensory trials accompanied by correct decisions (Fig. 3b,c). To
176 avoid any potent influence of the outcome-related activities, we calculated fluorescence
177 changes during the stimulus period before the outcomes (0 ~ 1 s). In the stationary sessions,
178 many of the PPC excitatory neurons were identified as visual-only (41.7%) or multisensory
179 responsive neurons (36.7%), but relatively small portion of them were auditory-only
180 responsive neurons (10.6%) (Fig. 2c). In the moving sessions, the proportion of visual neurons
181 increased (54.7%), and many neurons lost their auditory responses (Fig. 3c,d and
182 Supplementary Fig. 2a). When we compared the response amplitudes of the PPC neurons, the
183 auditory responses were significantly reduced during locomotion. Still, the visual responses
184 were similar between the stationary and the moving states (Fig. 3d). This finding indicates that
185 locomotion selectively degrades auditory, but not visual responses in the PPC of task-
186 performing mice.

187 During the task, mice often started to lick within the stimulus period, and the stimulus-
188 evoked activity of the PPC neurons might be mixed with the licking-evoked activities during
189 the stimulus presentation period. To decompose the PPC population activity into specific
190 activities representing sensory stimulus, licking decisions, stimulus-decision interactions, or
191 other independent factors, we used demixed principal component analysis (dPCA)[72]. We fed
192 neural data from unisensory trials (i.e., A_G, A_{NG}, V_G, V_{NG} with licking or no-licking decisions)

193 for the dPCA (Fig. 3e). We confirmed that the decomposed PPC activity in the stimulus PC
194 axes reliably represented each stimulus information regardless of licking actions after the
195 stimuli (Supplementary Fig. 2b). On the other hand, dPCA properly dissociated decision-
196 relevant activity in the PPC neurons in other axes (Supplementary Fig. 2c,d). Interestingly, the
197 stimulus axis explained the PPC population activity much more than any other axes in both
198 stationary and moving conditions (Fig. 3f and Supplementary Fig. 2e), indicating that the PPC
199 neurons represent sensory information the most strongly during the task.

200 We next examined how the PPC activity represented auditory and visual Go/No-go
201 stimuli in the stimulus subspace by comparing trial-averaged neuronal trajectories of each
202 unisensory stimulus in the top three PCs (Fig. 3g; mean % explanation by top three stimulus
203 PCs: 62.8%). First, we quantitatively measured the magnitude of sensory representations by
204 calculating the projection distance of each trajectory during the stimulus presentation period
205 (for 1 s after stimulus onset) (Fig. 3g; Methods). Auditory trajectories were much shorter than
206 visual trajectories and became even shorter as animals made longer locomotion (Fig. 3h). Next,
207 we calculated the Euclidean distance between a pair of trajectories to quantify similarities in
208 the representation of each stimulus type (Fig. 3i and Supplementary Fig. 2f). Auditory Go and
209 No-go trajectories were close to each other and less distinct during locomotion (Fig. 3i). In
210 contrast, visual Go and No-go trajectories were divergent and distinct from each other (Fig. 3i).
211 The visual trajectories also differed from the auditory trajectories (Supplementary Fig. 2f).
212 Finally, to understand the trial-by-trial reliability of unisensory representation in the PPC, we
213 developed a classifier, which predicted the presented stimulus type in the current trial based on
214 the Euclidean distance between the current-trial trajectory and the trial-averaged trajectory (Fig.
215 3j). Classification accuracies were significantly higher for the visual trials than the auditory
216 trials (Fig. 3k,l). Moreover, accuracies of auditory classification were significantly lower in the
217 moving sessions than in the stationary sessions (Fig. 3l). Collectively, the PPC neurons

218 processed task-relevant visual information more strongly than the auditory information,
219 showing robust visual but weak auditory Go/No-go discrimination. More importantly,
220 locomotion further dampened the auditory representation in the PPC.
221
222 **Multisensory representation in the PPC determines the dominant modality for perceptual**
223 **decisions under audiovisual conflict**
224 We next examined how the PPC neurons represent multisensory information by
225 projecting their activity into the stimulus subspace during the multisensory trials (Fig. 4a,b;
226 Methods). The neural trajectories representing the congruent multisensory stimuli were very
227 close to the visual trajectories but highly distinct from the auditory trajectories in both
228 stationary and moving conditions (Fig. 4a,b). Euclidean distances, projection distances, and
229 classifier accuracies between the congruent Go and No-go trajectories were not different from
230 those between the visual Go and No-go trajectories regardless of locomotion conditions
231 (Supplementary Fig. 3a-d). These findings suggest that PPC neurons represent congruent
232 multisensory inputs in a similar way that they do visual stimuli.
233 By projecting PPC activity trajectories during incongruent multisensory trials, we
234 found that PPC neurons represented the same stimulus condition ($A_{NG}V_G$ or A_GV_{NG}) differently
235 depending on the impending decisions of mice (Fig. 4c; auditory dominance in grey trajectories
236 vs. visual dominance in black trajectories). We first found that the projection and the Euclidean
237 distances of the trajectories for auditory-dominant incongruent trials were smaller than those
238 for the visual-dominant trials (Supplementary Fig. 3e,f). Furthermore, the trajectories
239 representing the incongruent stimuli were nearly identical to those representing visual stimuli
240 when mice made visually dominant decisions (Fig. 4d and Supplementary Fig. 3g). When mice
241 made auditory-dominant decisions, however, the neural trajectories for the incongruent stimuli

242 diverged from the visual trajectories, becoming closer to but still separate from the auditory
243 trajectories (Fig. 4d and Supplementary Fig. 3g).

244 We next classified the incongruent trials individually by calculating the Euclidean
245 distance between the single-trial trajectory and the mean trajectories of the four types of
246 multisensory trials and found that the classification accuracy was significantly higher in the
247 stimulus subspace than in other subspaces (Supplementary Fig. 3h). Therefore, the sensory
248 representation in the PPC is the most critical factor determining the multisensory decisions of
249 mice in the audiovisual conflict during the task. We further developed another classifier by
250 setting the boundary of the visual trajectories based on their trial-by-trial variations and
251 classified individual incongruent trajectories as visually dominant ones if they were within the
252 boundary of the visual trajectories (Fig. 4e). Using this, we successfully classified the dominant
253 modality across incongruent trials (Fig. 4f). Collectively, if the PPC neurons dominantly
254 represented visual information under incongruent audiovisual stimuli, mice showed visually
255 dominant decisions. Conversely, if the visually dominant representation weakened in the PPC,
256 mice made auditory-dominant decisions in response to the incongruent stimuli.

257 To understand if the stimulus representation in the PPC changes with locomotion, we
258 calculated the divergence between the incongruent multisensory trajectory and the visual
259 trajectory at different locomotion states (Fig. 4g). The two trajectories were closer as the animal
260 made longer locomotion, and this was correlated with the decrease in auditory dominance rates
261 in the animal's multisensory decisions (Fig. 4g). To understand how locomotion altered the
262 trial-averaged neural trajectories in incongruent trials, we further compared the response
263 amplitudes by calculating the absolute values of stimulus-evoked responses in visual- or
264 auditory-responsive neurons across different locomotion and stimulus conditions. Responses
265 of visually responsive neurons were strongly suppressed only in auditory-dominant trials,
266 regardless of locomotion (Fig. 4h top). In contrast, auditory-responsive neurons exhibited

267 stronger responses in auditory-dominant trials compared to visual-dominant trials, while their
268 auditory responses gradually decreased during locomotion (Fig. 4h bottom). Therefore,
269 locomotion increased the likelihood of maintaining strong visual representation while reducing
270 the auditory representation in the PPC and caused mice to make more visually dominant
271 multisensory decisions.
272
273 **Locomotion selectively suppresses auditory cortical outputs to the parietal cortex but not**
274 **to the striatum**
275 The robust reduction of auditory representation in the PPC during locomotion might
276 be due to direct suppression of the auditory neurons in the PPC or indirect suppression of the
277 AC output neurons that project to the PPC (i.e. AC_{PPC} neurons). To examine which case it was,
278 we measured the spontaneous activity changes in the PPC auditory-responsive neurons during
279 locomotion. Neither the locomotion onset nor offset induced significant suppression in their
280 activities (Supplementary Fig. 4a-d). Therefore, the suppression of the auditory responses in
281 the PPC during locomotion is unlikely to result from direct inhibition of the PPC auditory
282 neurons. Instead, it might be due to the reduction of bottom-up auditory inputs to the PPC.
283 To examine this, we first traced the AC_{PPC} neurons by injecting the retrograde adeno-
284 associated viruses (AAVrg) encoding tdTomato into the PPC (Fig. 5a). We co-traced the AC
285 neurons that project to the posterior striatum (AC_{STR}), which are known to play a critical role
286 in the auditory decision-making of mice[73-76], by injecting the AAVrg encoding eGFP into the
287 striatum (Fig. 5a). AC_{PPC} neurons were mostly found in the anterior and dorsal AC (AuD),
288 whereas AC_{STR} neurons were found across the anterior-to-posterior and dorsal-to-ventral AC
289 (Fig. 5b,c). Only 7% of the traced neurons in the AC were co-labeled, suggesting that the AC_{PPC}
290 and the AC_{STR} neurons are distinct and non-overlapping neuronal populations in the AC (Fig.
291 5d).

292 We next measured the activity of AC_{PPC} and AC_{STR} neurons in mice running on the
293 treadmill (Fig. 5e,k). When animals started to move, the spontaneous activity of AC_{PPC} neurons
294 was significantly reduced, and their calcium activities and locomotion onset speeds were
295 negatively correlated (Fig. 5f). AC_{PPC} neurons were liberated from the inhibition at locomotion
296 offset (Fig. 5g). Unlike the AC_{PPC} neurons, AC_{STR} neurons did not exhibit any activity changes
297 at the onset or offset of locomotion (Fig. 5l,m). These results demonstrate that locomotion
298 suppressed AC_{PPC} neurons directly and selectively without inhibiting AC_{STR} neurons.
299 We next measured auditory responses in AC neurons across different locomotion
300 states (Supplementary Fig. 5a). Locomotion significantly suppressed the auditory responses of
301 AC_{PPC} neurons but not AC_{STR} neurons (Supplementary Fig. 5b and 5d). When we calculated
302 the stimulus selectivity between the 5kHz and 10kHz tones used for the training, only AC_{STR}
303 neurons showed a significant increase in selectivity during locomotion (Supplementary Fig. 5c
304 and 5e). These data suggest that locomotion selectively suppresses auditory responses in AC_{PPC}
305 neurons while enhancing stimulus selectivity in AC_{STR} neurons, which may be responsible for
306 improved auditory discrimination during locomotion (Fig. 1f).
307 We also measured visual responses in VC neurons during locomotion (Supplementary
308 Fig. 5f). We identified VC neurons that project to the PPC (VC_{PPC}) through retrograde labeling
309 with tdTomato while imaging all VC excitatory neurons in CaMKIIα::GCaMP6f mice using a
310 2-photon microscope (see Methods). Consistent with previous reports[29,31], overall VC neurons
311 exhibited increased visual responses and enhanced stimulus selectivity during locomotion
312 (Supplementary Fig. 5g-j). The increased visual responses and stimulus selectivity in VC
313 neurons, including VC_{PPC}, may explain the observed improvement in visual discrimination
314 during locomotion. Collectively, our findings indicate that locomotion differentially modulates
315 stimulus-evoked activity in AC and VC neurons, potentially influencing auditory and visual
316 discrimination as well as audiovisual integration.

317

318 **Locomotion reduces task-relevant auditory representation in the AC_{PPC} neurons**

319 We next examined the stimulus-evoked activities of AC_{PPC} and AC_{STR} neurons during
320 the task. Both AC_{PPC} and AC_{STR} neurons showed significant auditory responses but no
321 profound visual responses during the task (Supplementary Fig. 6a-c and Supplementary Fig.
322 7a-c). Prolonged locomotion suppressed the auditory responses of the AC_{PPC} neurons
323 (Supplementary Fig. 6c). In incongruent trials, AC_{PPC} neurons showed strong responses when
324 animals made auditory-dominant decisions but significantly weak responses during visually-
325 dominant decisions (Fig. 5h,i). Locomotion-induced suppression of the AC_{PPC} neurons was
326 correlated with reduced auditory dominance in multisensory decisions of mice (Fig. 5j).
327 However, there was no such suppression in the AC_{STR} neurons during locomotion, and the
328 population of AC_{STR} neurons showed auditory responses at similar levels across the trials
329 independent of locomotion conditions and dominant modalities (Fig. 5n-p and Supplementary
330 Fig. 6c).

331 We further analyzed AC population activity using the dPCA. As shown in the PPC
332 neurons, the stimulus axis explained the activities of both AC subpopulations more strongly
333 than other task-relevant axes (mean % explanation by top three stimulus PCs: 53.6% for AC_{PPC}
334 neurons; 42.2% for AC_{STR} neurons). During locomotion, the auditory trajectories significantly
335 shrank only in the AC_{PPC} neurons (Supplementary Fig. 6d-f), but not in the AC_{STR} neurons
336 (Supplementary Fig. 7d-f). Furthermore, only AC_{PPC} neurons showed decreased classification
337 accuracies for the auditory stimuli during locomotion (Supplementary Fig. 6g and
338 Supplementary Fig. 7g). During incongruent trials, the response amplitudes and the neural
339 trajectories of the AC_{PPC} neurons were significantly smaller in the visual-dominant trials than
340 in the auditory-dominant trials (Supplementary Fig. 6h-j). In contrast, AC_{STR} neurons showed
341 consistent responses to the incongruent stimuli regardless of dominant modalities

342 (Supplementary Fig. 7h-j). These data indicate that locomotion suppressed the AC_{PPC} neurons
343 more than AC_{STR} neurons, and this selective suppression switched mice to make visually
344 dominant decisions in incongruent trials. In contrast to the vulnerability of the AC_{PPC} neurons,
345 AC_{STR} neurons were unaffected by locomotion, suggesting that the AC_{STR} neurons reliably
346 encode auditory information even during locomotion and are unrelated to multisensory
347 decisions influenced by the locomotion.
348

349 **Optogenetic double dissociation reveals distinct roles of the AC subpopulations in**
350 **perceptual decisions during the audiovisual discrimination task**

351 We wondered whether the two distinct AC outputs, AC_{PPC} and AC_{STR}, play distinct
352 functional roles during the audiovisual discrimination task. We first examined whether the
353 activity in the AC_{PPC} neurons was required for auditory dominance in multisensory decisions
354 of mice during incongruent trials. We expressed halorhodopsin (eNpHR3.0) in AC_{PPC} neurons
355 and optogenetically inhibited them in task-performing mice (Fig. 6a). Optogenetic inhibition
356 of the AC_{PPC} neurons did not affect the mice's decisions in auditory, visual, and congruent
357 audiovisual trials (Fig. 6b). However, it caused a significant reduction in auditory-dominant
358 decisions in stationary mice (Fig. 6b).

359 We next examined the role of AC_{STR} neurons during the task by optogenetic inhibition
360 of those neurons (Fig. 6c). Similar to previous studies[73,74], inhibition of the AC_{STR} neurons
361 significantly hampered auditory discrimination in stationary mice (Fig. 6d). In correlation with
362 a decrease in auditory discrimination, inactivation of AC_{STR} also led to a reduction in auditory-
363 dominant decisions during incongruent trials (Fig. 6e,f). Our findings indicate that the AC-to-
364 STR circuit is important for auditory-dependent perceptual decisions (Fig. 6c,d,f), whereas the
365 AC-to-PPC circuit is more crucial for making auditory-dominant decisions under audiovisual
366 conflicts (Fig. 6a,b,e).

367

368 **The auditory cortical inputs inhibit visual representation in the PPC**

369 We next investigated whether AC_{PPC} neurons can suppress visual responses in the PPC
370 during incongruent trials. To address this, we conducted calcium imaging of the PPC excitatory
371 neurons in stationary mice while optogenetically inhibiting AC axons using a miniature
372 fluorescence microscope combined with an optogenetic manipulation system (nVoke; Fig. 7a).
373 Optogenetic inhibition of AC axon terminals in the PPC significantly suppressed auditory
374 responses but did not affect visual responses in the PPC neurons (Fig. 7b). This result indicates
375 that optogenetic inhibition of AC axons in the PPC selectively reduced auditory inputs to the
376 PPC. Next, we compared the response amplitudes of visually responsive PPC neurons between
377 LED-off and LED-on conditions during incongruent trials. As expected, inhibition of AC
378 inputs significantly increased visual responses in the PPC visual neurons (Fig. 7c). Optogenetic
379 inhibition of AC_{PPC} axon terminals also resulted in a significant decrease in auditory-dominant
380 decisions during incongruent trials in stationary mice (Fig. 7d), similar to the effect observed
381 during somatic inhibition of AC_{PPC} neurons (Fig. 6a,b). Collectively, our findings indicate that
382 the AC-to-PPC projection inhibits visual neurons in the PPC, promoting auditory dominance
383 in animals' decisions during audiovisual conflicts in a stationary state. In contrast, locomotion
384 induces more visually dominant decisions by gating the AC-to-PPC circuit.

385

386 **Motor cortical projection to the AC suppresses AC_{PPC} neurons during locomotion**

387 Previous research reported that the neural projection from the M2 to the AC suppressed
388 auditory responses of AC neurons[37,38]. Our data further showed that locomotion suppressed the
389 AC_{PPC} neurons but not the AC_{STR} neurons. To examine if the M2 mediates this selective
390 suppression of the AC_{PPC} neurons, we first anatomically mapped the spread of fluorescence-
391 labeled M2 axons in the AC (Fig. 8a). Similar to the previous report[37], M2 axons primarily

392 innervated the superficial or deep layers of the AuD (Fig. 8b). When we compared the M2 axon
393 distribution with the distributions of the AC_{PPC} and the AC_{STR} neurons across AC areas, M2
394 axons were localized at a similar location where the AC_{PPC} neurons were found (Fig. 8b). On
395 the other hand, majority number of the AC_{STR} neurons did not overlap well with the M2 axons
396 (Fig. 8b). This anatomical feature of the overlap between the M2 axons and the AC_{PPC} neurons
397 in the AuD suggests potential modulation of the AC_{PPC} neurons by the M2 during locomotion.
398 We then examined whether this M2 activity suppressed AC_{PPC} neurons directly
399 without affecting AC_{STR} neurons. Using the nVoke system, we activated M2 axon terminals in
400 the AC while imaging calcium activity in AC subpopulations (Fig. 8c). Optogenetic activation
401 of M2 axons significantly dampened the auditory responses of AC_{PPC} neurons (Fig. 8d). In
402 contrast, AC_{STR} neurons were unaffected by M2 axon activation and showed consistent
403 auditory responses during M2 axon activation (Fig. 8d). This result indicates that activation of
404 M2 axons in the AC selectively mediates the suppression of AC_{PPC} neurons.
405 Next, we investigated whether the activity of M2 neurons that project to the AC
406 correlates with the dominant modality in incongruent trials as well as with locomotion. We first
407 measured the calcium activity of AC-projecting M2 neurons ($M2_{AC}$) in mice performing the
408 task in the stationary condition (Fig. 8e). Interestingly, as shown in the peri-stimulus histogram,
409 $M2_{AC}$ neurons exhibited higher activity in visual-dominant trials compared to auditory-
410 dominant trials (Fig. 8f,g). This result suggests that trial-by-trial variations in the spontaneous
411 activity of $M2_{AC}$ neurons, even before stimulus onset, determine the dominant modality during
412 audiovisual conflicts.
413 We then measured the calcium activity of $M2_{AC}$ neurons in mice running on the
414 treadmill. $M2_{AC}$ neurons showed robust activation at locomotion onset (Fig. 8h), and the
415 calcium activity of these neurons was significantly higher during the later period of locomotion

416 compared to immediately after locomotion onset (Fig. 8i). This result indicates that M2 neurons
417 copied and delivered the locomotion onset signal to the AC.

418 Lastly, we optogenetically inhibited the M2 axon terminals in the AC in mice
419 performing the task (Fig. 8j) and found that it did not alter the animal's decisions in unisensory
420 or congruent trials (Fig. 8k). However, it significantly enhanced auditory dominance in
421 incongruent trials during locomotion (Fig. 8k). These results strongly support the idea that
422 locomotion raises the activity of the M2-to-AC circuit[38], and we further found that the
423 locomotion-induced activation of this cortical circuit selectively inhibits the AC outputs to the
424 PPC. Consequently, PPC activity is dominated by visual information during locomotion,
425 leading to more visually dominant decisions in mice facing audiovisual conflicts (Fig. 9).
426

427 **Discussions**

428 In this study, we identified a neural mechanism underlying behavior state-dependent changes
429 in sensory dominance during multisensory decision-making under audiovisual conflicts in mice.
430 Auditory cortical outputs to the parietal cortex inhibited visual representations in the PPC,
431 leading to auditory-dominant decisions. These auditory outputs were suppressed by locomotion,
432 resulting in more visually dominant decisions. Interestingly, locomotion did not suppress
433 auditory outputs to the STR, allowing animals to maintain precise auditory decisions even
434 during locomotion. Our findings demonstrate that top-down projections from the M2 to the AC
435 selectively gate auditory cortical outputs to the higher association cortex. This gating
436 mechanism specifically regulates how the PPC represents audiovisual conflicts while
437 maintaining accurate perceptual decisions in auditory-only environments in behaving animals.

438 As all animals naturally locomote while collecting sensory information in the
439 environment to make decisions, understanding the role of locomotion in perceptual decision-
440 making is ethologically critical. More recently, perceptual experiments for head-fixed mice on

441 the treadmill were devised[31]. Using this system, previous studies have examined the effects of
442 locomotion on the simple perceptual detections under the unisensory (either visual or auditory)
443 condition[27,35,39], but the effect of locomotion on the discrimination of different modality inputs
444 and multisensory decision-making has never been tested. Our study designed a behavioral
445 paradigm to measure perceptual decision-making performances in the unisensory (visual or
446 auditory) and multisensory (congruent or incongruent) conditions at different locomotion states
447 within one session in the same animal. We found that locomotion can improve both visual and
448 auditory perceptual decisions after discrimination of salient stimuli in the same animal. This
449 might be due to the increased stimulus selectivity and sensory responses in the sensory cortices
450 (Supplementary Fig. 5), which can potentially enhance visual and auditory discriminability in
451 animals[34,77].

452 We further found that locomotion can switch multisensory decisions from auditory-
453 dominant to visual-dominant ones in mice. The effect of locomotion on multisensory
454 perception and decision has never been examined before. Our findings demonstrate that the
455 dominant modality can be flexibly switched from audition to vision depending on the
456 locomotion states. Sensory dominance in multisensory decisions can be beneficial for animals
457 to make rapid perceptual decisions[78], which is critical for the survival of animals in a
458 complicated world. Depending on the task design, specific sensory modality information
459 provides more reliable information than other modalities during multisensory integration[78]. A
460 more reliable sensory modality can provide a stronger effect on multisensory decisions in
461 animals performing the task. For example, visual information is more critical for animals to
462 discriminate spatial locations of the multisensory stimuli[9], while auditory information is more
463 important for temporal discrimination of the stimuli[79]. Our study suggests that the locomotion
464 condition of an animal can flexibly switch the appropriate modality even during the same task.
465 The determination of the dominant modality has been explained by Bayesian models, which

466 explain the optimal strategy of re-weighting different sensory inputs based on their reliability
467 (or variance)[10,11,14]. Our data further suggest that the locomotion generates a self-initiated
468 internal signal that can change the relative weights of the auditory inputs compared to the visual
469 inputs by lowering the reliability of the auditory information in the parietal cortex, where the
470 dominant modality is determined.

471 Locomotion increases corollary discharge signals in the M2, potentially degrading
472 auditory representations in the AC[38,80]. We further found that locomotion-evoked suppression
473 of auditory responses only happened in the auditory-to-parietal projection (AC_{PPC} neurons)
474 without impairing auditory responses in the auditory-to-striatal projection (AC_{STR} neurons)
475 (Fig. 5 and Supplementary Fig. 6,7). Therefore, corollary discharge signals evoked by
476 locomotion weaken a specific auditory flow from the AC to the higher association cortex. The
477 distinct roles of AC outputs may enable the mammalian brain to maintain auditory processing
478 during locomotion to make auditory-dependent decisions accurately while switching the
479 dominant modality and relying less on auditory stimuli during multisensory decisions under
480 the audiovisual conflicts.

481 Interestingly, we also found that $M2_{AC}$ neurons exhibited spontaneous activity
482 fluctuations that correlated with visual dominance rates even in stationary mice (Fig. 8e-g).
483 This activity fluctuation may reflect internal state changes that are independent of actual motor
484 output before locomotion or other unmeasured motor behaviors in head-fixed mice. Future
485 studies are required to determine whether M2 activation specifically inhibits the dorsal AC,
486 where AC_{PPC} neurons are located, by forming specific top-down inhibitory synaptic
487 connections, rather than affecting other cortical areas or neurons.

488 In contrast to auditory representation in the PPC, we found that locomotion did not
489 significantly weaken or strengthen visual representation in the PPC (Fig. 3). However, some
490 individual neurons reshaped their visual responsiveness (either increased or decreased,

491 Supplementary Fig. 2a) during locomotion. Furthermore, most VC neurons showed enhanced
492 visual responses and stimulus selectivity during locomotion (Supplementary Fig. 5f-j), possibly
493 due to cholinergic activation in the VC[29]. This improved visual processing may lead to better
494 visual discrimination during locomotion. However, the increase in visual dominance during
495 multisensory trials was independent of enhanced visual discrimination during locomotion
496 (Supplementary Fig. 1c), suggesting that these two modulations occur in parallel via different
497 pathways.

498 Consistent with previous research[48], we found the PPC excitatory neurons represent
499 visual information more reliably than auditory information during the task. Although we
500 observed more visually responsive neurons than auditory-responsive neurons in the PPC, our
501 previous study showed balanced auditory and visual responses in the PPC (see Fig. 7 of
502 reference[12]). This difference was mainly due to increased visual responses in PPC neurons
503 compared to the previous study. The increased portion of visual neurons in this study might be
504 attributed to differences in stimulus types (complex drifting grating vs. optogenetic cortical
505 stimulation and flash), task-learning states (expert vs. naïve mice), and anesthesia states (awake
506 and task-engaged vs. anesthetized) between the current and previous studies. Despite this
507 discrepancy, both studies agree that strong auditory inputs to the PPC can disrupt its visual
508 representation, thereby facilitating auditory-dominant multisensory decisions in head-fixed,
509 stationary mice.

510 Interestingly, PPC excitatory neurons discriminated auditory Go/No-go information
511 during auditory-based decisions less effectively than visual information, suggesting that the
512 PPC itself is not involved in auditory decision-making. Supporting this, when we inactivated
513 the PPC either through muscimol injection or strong optogenetic activation of PV^+ inhibitory
514 interneurons, we observed impairments in visual discrimination but not auditory discrimination
515 behaviors. Therefore, the PPC is more critical for visual decision-making in mice. Under

516 multisensory conditions, the PPC integrates auditory inputs that can negatively impact visual
517 weighting, and such integration is necessary for auditory-dominant multisensory decisions in
518 incongruent trials. We also found that the AC output to the STR, which is important for auditory
519 decision-making, exhibited stable auditory representation even during visually dominant
520 decisions (Fig. 5 and Supplementary Fig. 7). Future studies are required to fully understand
521 whether the strong visual representation in the PPC is also required to suppress downstream
522 areas of AC_{STR} neurons to shift auditory-dominant decisions to visually dominant ones. This
523 unknown circuit might be responsible for the visual dominance observed when the PPC was
524 inactivated, as discussed in our previous study[12].

525 Our data also indicate that the suppression of visual responses in the PPC only occurs
526 in incongruent trials (not congruent trials) when animals make auditory-dominant decisions
527 (Fig. 4h). One potential explanation for this congruency-dependent cross-modal suppression
528 would be an antagonistic selectivity between Go and No-go stimuli in auditory-to-visual
529 inhibitory circuits. Supporting this idea, opponent inhibition between choice-selective neurons
530 was recently found in the PPC[81]. Our previous report showed that PV^+ neurons in the PPC
531 strongly received AC inputs and mediated auditory-dominant behaviors[12]. Future studies are
532 required to examine whether the selectivity of inhibitory neurons emerges with learning in
533 these inhibitory neurons in the PPC. Similar to the role of the mouse PPC exerting cross-modal
534 inhibition, the human prefrontal cotex[82] and the superior temporal sulcus[17,83] also showed
535 multisensory depression in resolution of conflicting audiovisual speech stimuli. Therefore,
536 multisensory depression might happen across association areas when animals face
537 multisensory conflicts, and our study demonstrates how locomotion states flexibly adjust such
538 inhibition during multisensory conflicts by gating bottom-up inputs.

539 **Methods**

540 **Animals and surgery**

541 *Animals*

542 All experimental procedures were approved by the KAIST Institutional Animal Care
543 and Use Committee (IACUC-18-100, IACUC-18-235). Both male and female mice (P45-P150)
544 were used in this study. Animals were maintained *ad libitum* under light (8 am-8 pm) and dark
545 cycle (8 pm-8 am) conditions and housed under single animal per cage conditions from the
546 start until the last day of the experiment (temperature: 20 ~ 22°C; humidity: 30 to 50%). We
547 used C57BL/6J wild-type (WT) mice, B6;129P2-Pvalb$^{tm1(cre)Arbr}$/J mice (PV-IRES-Cre, stock
548 no. 008069, Jackson Laboratory), B6.Cg-Tg(Camk2a-cre)T29-1Stl/J mice (CaMKIIα-Cre,
549 stock no. 005359, Jackson Laboratory), Ai148 mice (stock no. 030328, Jackson Laboratory)
550 crossed with the CaMKIIα-Cre mice, and Ai162 mice (stock no. 031562, Jackson Laboratory).

551

552 *Common procedure of animal surgery*

553 Adult mice (P45-P80) were anesthetized with isoflurane (1.5%–2% in oxygen) and
554 fixed their head on the stereotaxic apparatus. The body temperature was monitored and
555 maintained at 37°C using a heating pad connected to a body temperature sensor. The scalp was
556 alternately sterilized three times with 70% ethanol and povidone-iodine solution. After the
557 sterilization of the scalp, surgical scissors was used to cut the scalp according to the midline
558 (for virus injection) or remove a portion of the scalp (for the implantation of head plates, GRIN
559 lens, and optic fiber). Periodsteum above the skull was removed, and povidone-iodine solution
560 was used to sanitize the exposed skull and incision. Lastly, we cleaned the exposed skull with
561 sterilized phosphate-buffered saline (PBS).

562

563 *Virus injection for retrograde tracing*

564 For the retrograde tracing of the AC neurons that project to the PPC and the STR, we
565 injected 0.5 μl of retrograde AAV expressing tdTomato (AAVrg-CAG-tdTomato, Addgene)
566 and 0.5 μl of retrograde AAV expressing GFP (AAVrg-CAG-GFP, Addgene) into the target
567 areas respectively. After 2~3 weeks from the injections, we perfused mice to collect the brain
568 samples for histology.
569
570 *Head plate implantation surgery for mouse head-fixation*
571 To implant a stainless steel head-plate on the mouse head, three miniature stainless
572 steel screws (J.I. Morris) were implanted into the exposed skull using cyanoacrylate glue
573 (Loctite super glue 401, Henkel). A customized stainless steel head-plate was attached to the
574 skull with the cyanoacrylate glue, and the between the skull and head-plate was filled by dental
575 acrylic (Ortho-Jet, Lang Dental).
576
577 *Surgical procedures for in vivo calcium imaging with miniature microscope*
578 To express GCaMP6s in the target neurons, we made a small craniotomy (diameter
579 ~0.5 mm) above the targeted location. To conduct *in vivo* calcium imaging at the PPC, we
580 injected ~0.5 μl of Cre-recombinase dependent adeno-associated virus (AAV) expressing
581 GCaMP6s (AAV5-Syn-Flex-GCaMP6s-WPRE-SV40, UPENN) into a site that is 0.2 mm
582 away from the right PPC in posterior direction (posterior 2.15 mm, lateral 1.6 mm from bregma;
583 depth 0.35 mm) of CaMKIIα-Cre mice using a thin pulled glass pipette (20~25 μm of tip
584 diameter, item no. 504949, WPI) installed in a Nanoliter 2010 injector (WPI) at a speed of 24
585 nl/min. For *in vivo* calcium imaging of AC_{PPC} neurons, we injected ~0.5 μl of retrograde AAV
586 expressing GCaMP6s (AAVrg-hSyn1-GCaMP6s-P2A-nls-dTomato, Addgene) into the right
587 PPC (posterior 1.95 mm, lateral 1.6 mm from bregma; depth 0.35 mm) of the WT mice. For *in*
588 *vivo* calcium imaging of AC_{STR} neurons, we injected ~0.5 μl of retrograde AAV expressing

589 GCaMP6s (AAVrg-hSyn1-GCaMP6s-P2A-nls-dTomato, Addgene) into the right STR
590 (posterior 1.5mm, lateral 3.45mm from bregma; depth 2.8mm) of the WT mice. For *in vivo*
591 calcium imaging of AC-projecting M2 neurons, we injected ~0.5 μl of retrograde AAV
592 expressing Cre-recombinase (AAVrg-hSyn-Cre, Addgene) into the right AC (posterior 2.5mm,
593 lateral 4.2mm from bregma; depth 0.8mm) of the Ai162 mice. For *in vivo* calcium imaging of
594 the PPC neurons with optogenetic inhibition of AC axons with nVoke system (Inscopix), we
595 injected ~0.5 μl of AAV5-Syn-Flex-GCaMP6s-WPRE-SV40 into the right PPC (posterior 2.15
596 mm, lateral 1.6 mm from bregma; depth 0.35 mm) and injected Cre-recombinase-dependent
597 AAV expressing eNpHR3.0-mCherry (AAV2-EF1α-DIO-eNpHR3.0-mCherry, UNC Vector
598 Core) into the right AC. For *in vivo* calcium imaging of AC neruons with optogenetic of M2
599 axons with nVoke system, we injected ~0.5 μl of retrograde AAV expressing Cre recombinase
600 into the right PPC or STR and ~0.5 μl of AAV-hSyn-ChrimsonR-tdTomato (Addgene) into the
601 right M2 at two anterior-posterior coordinates (anterior 1.0 & 1.7 mm, lateral 0.75 mm from
602 bregma; depth -0.6 mm) of Ai162 mice. After the injection, the incision was sutured with a
603 stitching fiber and disinfected with a povidone-iodine solution.

604 After 10-14 days from the virus injection, gradient reflective index (GRIN) lens
605 implantation surgery was conducted as previously demonstrated[84]. Mice received subcutaneous
606 injections of carprofen (5 mg/Kg) and dexamethasone (5 mg/Kg) 1 hour before the surgery.
607 After anesthetization of a mouse, a 1 mm^2 of square-shaped craniotomy was made on the skull
608 above the area of implantation. A prism-attached GRIN lens (1050-004601 or 1050-004606,
609 Inscopix) was inserted 0.2mm away from the imaging area, where we made a small linear
610 incision of the cortical surface using a surgical knife (10055-12, Fine Science Tools) coupled
611 to the stereotaxic apparatus. The GRIN lens was gently inserted (-0.1 mm/20 s, depth 0.8 mm
612 for the PPC; 1.4 mm for the AC; 1.1 mm for the M2) in different directions of the image plane
613 based on the target areas (PPC and AC: along the medial-lateral axis; M2: along the anterior-

614 posterior axis). The exposed brain tissue between the GRIN lens and skull was covered with
615 Kwik-Sil (WPI), and the inserted GRIN lens was secured by applying Super-Bond (Super-
616 Bond C&B Kit, Sun Medical Co.) and the cyanoacrylate glue over the cured Kwik-Sil layer
617 and connected skull. Mice were then implanted with the head plates. Mice were subcutaneously
618 injected with carprofen and dexamethasone for three days following surgery. The field of view
619 of each mouse was examined on a regular basis, and if we detected obvious neuronal activity,
620 we fastened a baseplate (1050-004638, Inscopix) atop the GRIN lens using dental acrylic. To
621 protect the lens from dirt, the baseplate was covered with a baseplate cover (1050-004639,
622 Inscopix).
623
624 *Surgical procedures for in vivo calcium imaging with 2-photon microscope*
625 We injected 0.5 μl of retrograde AAV expressing tdTomato (AAVrg-CAG-tdTomato,
626 Addgene) into the right PPC of cross-line mice (Ai148 x CaMKIIα-Cre). 10~14 days later,
627 craniotomy and head-plate implantation surgery were conducted as previously demonstrated[85].
628 Mice received subcutaneous injections of carprofen (5 mg/Kg) and dexamethasone (5 mg/Kg)
629 1 hour before the surgery. After the anesthetization of a mouse, a round craniotomy with a 3
630 mm diameter was made on the right posterior cortical area. A 3-layered round cover glass,
631 which was made of 2 pieces of 3-mm-diameter cover glass (W4 64-0720, Warner Instruments)
632 and 1 piece of 5-mm-diameter cover glass (W4 64-0700, Warner Instruments) stacked by an
633 optical adhesive (no. 71, Norland products), was inserted into the craniotomy, and the edge of
634 the glass window was glued with VetBond (B00016067, 3M) and Super-Bond. Mice were then
635 implanted with the head plates. Mice were subcutaneously injected with carprofen and
636 dexamethasone for three days following the surgery.
637
638 *Surgical procedure for optogenetic manipulation during behavior task*

639 For optogenetic activation of PV^+ neurons in the right PPC, we injected 0.5 μl of Cre-
640 recombinase-dependent AAV expressing ChR2-eYFP (AAV2-EF1a-DIO-hChR2-ETTC-
641 eYFP, UNC Vector Core) or eYFP (AAV2-EF1a-DIO-eYFP, UNC Vector Core) into the PPC.
642 For optogenetic inhibition of projection-specific AC neurons, we bilaterally injected retrograde
643 AAV expressing Cre-recombinase (AAVrg-hSyn-Cre-WPRE-hGH, Addgene) into the right
644 PPC or bilateral STR (0.5 μl per each site) and 0.5 μl of Cre-recombinase-dependent AAV
645 expressing eNpHR3.0-mCherry (AAV2-EF1a-DIO-eNpHR3.0-mCherry, UNC Vector Core)
646 into the AC. For optogenetic inhibition of the M2-to-AC circuit, we injected the excitatory-
647 neuron-specific AAV expressing ChR2-eYFP (AAV2-CAMKIIa-ChR2-EYFP, UNC Vector
648 Core) or the AAV expressing eNpHR3.0-eYFP in neurons (AAV2-hSyn-eNpHR3.0-eYFP,
649 UNC Vector Core) into the right M2 at two anterior-posterior coordinates of WT mice (0.5 μl
650 per each coordinate). After the injection, mice were further implanted with the head plates.
651 Mice had 14 days of viral expression before starting water restriction for the behavioral
652 experiment. When mice were trained and ready for the manipulation experiment (see Methods;
653 **Behaviors**), we provided mice with sufficient water for 2 days and implanted optic fiber on
654 target sites for the laser light delivery. Mice were anesthetized with 1.5-2 % isoflurane, and a
655 0.5 mm-diameter craniotomy was made on the right AC. An optic fiber with a 200 μm diameter
656 was implanted into the right AC (0.6mm depth) and glued with Kwik-Sil and cyanoacrylate
657 glue. For the AC_{STR} inhibition (Fig. 6c), we implanted optic fibers into the AC bilaterally. We
658 recovered mice for three days after the surgery and restarted the water restriction and behavioral
659 training.
660
661 **Behaviors**
662 *Hardware setups for behavior experiments*

Visual stimuli were generated with a custom MATLAB code. A gamma-corrected LCD monitor (12 cm x 9 cm; minimal luminance: 0 lux; maximal luminance: 120 lux; refresh rate: 60Hz) was placed 10 cm away from the left eye of mice at a 45° angle from the rostral-caudal axis. For the binocular visual stimulation task, we put another monitor in front of the right eye of mice as we put on the left side. Full-field drifting gratings (100% contrast, 2 Hz temporal resolution, 0.04 cycles/° spatial resolution, 60 Hz refresh rate) were used for the visual discrimination task in two directions (rightward for Go; upward for No-go). Auditory stimuli were generated with a custom MATLAB code (sampling rate 119,000 Hz, 16bit). A speaker (#60108, Avisoft) was placed 10cm away from the left ear of the mice. Pure tones with different frequencies (10 kHz for Go, 5 kHz for No-go in the main task) were used for the auditory discrimination task. All sound stimuli were calibrated to have a 76 dB sound pressure level (SPL) at the left ear of mice.

Licking behavior of task-performing mice was detected by a custom-made lickometer. We delivered water reward and air punishment via solenoid valves (EV-2-24, Clippard). All the hardware components were operated and controlled by Presentation (Neurobehavioral Systems) with USB data acquisition devices (USB-201, Measurement Computing). An optical mouse (G100s, Logitech) was placed beside a spinning disk of the treadmill. The rotation of the disk during locomotion was converted to digitalized signals by the optical mouse, and real-time locomotion speed was calculated by a customized LabView code (sampling rate: 40 Hz). If the speed exceeded the locomotion threshold (3 cm/s), a 5V-digital signal was sent to the Presentation software in real time through a USB data acquisition device (USB-6001, National Instruments) to present sensory stimuli during locomotion.

Behavioral training and multisensory discrimination experiments

687 Mice underwent water restriction (~1 ml of water per day) throughout the behavioral
688 experiment. The weight of mice under the water restriction was monitored throughout the
689 experiments and maintained at more than 75% of the initial body weight before the water
690 restriction. We calculated the correct rate, hit rate, false alarm (FA) rate, and auditory
691 dominance rate as follows:

692 $$(1)Correct\ rate\ (\%) = \frac{\#Hit\ trials + \#Miss\ trials}{\#Total\ trials} \times 100$$

693 $$(2)Hit\ rate\ (\%) = \frac{\#Hit\ trials}{\#Hit\ trials + \#Miss\ trials} \times 100$$

694 $$(3)FA\ rate\ (\%) = \frac{\#FA\ trials}{\#CR\ trials + \#FA\ trials} \times 100$$

695 $$(4)Auditory\ dominance\ rate\ (\%) = \frac{\#A_G V_{NG} \rightarrow A\ trials + \#A_{NG} V_G \rightarrow A\ trials}{\#Incon\ trials} \times 100$$

696 $$(5)Auditory\ dominance\ rate\ in\ A_G V_{NG} (\%) = \frac{\#A_G V_{NG} \rightarrow A\ trials}{\#A_G V_{NG}\ trials} \times 100$$

697 $$(6)Auditory\ dominance\ rate\ in\ A_{NG} V_G (\%) = \frac{\#A_{NG} V_G \rightarrow A\ trials}{\#A_{NG} V_G\ trials} \times 100$$

698 We used adjusted hit rate and FA rate to calculate d′ from behavior data to avoid infinite values
699 due to the 100% hit rate or 0% FA rate in some sessions.

700 $$(7)Adjusted\ hit\ rate\ (\%) = \frac{\#Hit\ trials + 0.5}{\#Hit\ trials + \#Miss\ trials + 1} \times 100$$

701 $$(8)Adjusted\ FA\ rate\ (\%) = \frac{\#FA\ trials + 0.5}{\#CR\ trials + \#FA\ trials + 1} \times 100$$

702 $$(9)\ d' = z(Adjusted\ hit\ rate) - z(Adjusted\ FA\ rate)$$

703 All mice were trained and tested through the following five steps:
704 1) reward conditioning, 2) stimulus conditioning, 3) audiovisual discrimination training, 4)
705 treadmill habituation; 5) audiovisual integration test
706 1) Reward conditioning: water-restricted mice received 0.8 μl of water reward whenever they
707 licked the water port. If mice did not show any spontaneous licking behavior within the first 3
708 minutes after the beginning of a session, we manually delivered water through the water port
709 until mice started to lick the water port. If mice got more than 0.8 ml of total water reward (>

710 1000 licks) within the first 20 minutes without manual water delivery, mice were moved to the
711 second step in the next session.
712 2) Stimulus conditioning: auditory go stimulus, visual go stimulus, and no stimulation trials
713 were pseudo-randomly presented in the proportion of 1:1:2. If mice licked the water port during
714 2 s of response window after the stimulus offset, 1 μl of water reward and 2 s of reward
715 consumption time were presented (hit). If mice did not lick the water port until the offset of the
716 response window (miss), 1 μl of water reward was delivered at the end of the response window
717 to encourage learning. If mice licked the water port during the no stimulation trial (FA), 6 s of
718 additional time-out period was given. We gave 4 s extra time for the inter-trial interval before
719 beginning the next trial. Task sessions automatically ended when mice consecutively missed
720 30 auditory- or visual-Go stimuli. When mice showed more than 80% hit rates for visual and
721 auditory go stimuli, mice were moved on to the third step in the next session.
722 3) Audiovisual discrimination training: 4 types of stimuli (auditory Go, auditory No-go, visual
723 Go, visual No-go) were pseudo-randomly presented in equal proportion. There was no water
724 reward in the miss trials, and 400 ms of air puff punishment was delivered to the right cheek
725 of mice with the time-out period (6 s) in the FA trials. Task sessions automatically ended when
726 mice consecutively missed 10 auditory- or visual-Go stimuli. If mice achieved correct rates
727 higher than 80% for both auditory and visual discrimination, we considered that the mice
728 learned the discrimination tasks.
729 4) Treadmill habituation: We first habituated mice to run on the treadmill during the task by
730 presenting the same auditory and visual stimuli when mice ran faster than a speed threshold (3
731 cm/s). If mice reached an expert level of discrimination (> 80% of correct rates) while showing
732 enough locomotion activity (> 400 trials within 1 hour), mice consecutively performed the task
733 in the stationary block on the immobilized treadmill and in the moving block on the free-
734 rotating treadmill during a single day in random order. If mice showed an expert level of

735 performance in both conditions, they were moved on to the final step. We conducted optic fiber
736 implantation surgery for the optogenetic manipulation experiments when animals passed this
737 step.
738 5) Audiovisual integration test: auditory, visual, congruent (A_GV_G, $A_{NG}V_{NG}$), and incongruent
739 (A_GV_{NG}, $A_{NG}V_G$) stimuli were pseudo-randomly presented in the proportion of 3:3:1:1 or
740 3:3:2:2 for the main behavioral test (3:3:1:1 for muscimol experiment). 3:3:2:2 (for optogenetic
741 experiments and *in vivo* calcium imaging), or 3:3:1:3 (*in vivo* calcium imaging) ratio was used
742 for the audiovisual integration test to reserve enough trial numbers. There was no water reward
743 and air puff punishment in incongruent trials. Mice conducted both stationary and moving
744 blocks in random order on a single day except for *in vivo* calcium imaging experiments (See
745 the section on *in vivo* calcium imaging experiments).
746 In moving sessions, we divided trials into two categories: start-moving trials and keep-
747 moving trials. If the average speed before the stimulus onset (-3 ~ -1.5 s) exceeded the speed
748 threshold (> 3 cm/s), that trial was classified as keep-moving. To evaluate the correlation
749 between locomotion speed and auditory dominance (Supplementary Fig. 1d), we categorized
750 keep-moving incongruent trials according to mean locomotion speed (3 ~ 9 cm/s, 9 ~ 15 cm/s,
751 and higher than 15 cm/s) before the stimulus onset (-1 ~ 0 s). We next determined the auditory
752 dominance rate for each category. To analyze the correlation between trial history and auditory
753 dominance (Supplementary Fig. 1e), we collected and calculated the auditory dominance rates
754 for the following trial sequences: 1) V_G or A_{NG} trial followed by $A_{NG}V_G$ trial, and 2) A_G or V_{NG}
755 followed by A_GV_{NG} trial during the moving sessions. We then estimated the auditory
756 dominance rate based on the modality of the previous trial. To find the relationship between
757 auditory dominance rate and pupil size, we averaged the maximum-normalized pupil size
758 before the stimulus onset (-1 ~ 0 s) during moving sessions. We then calculated the average
759 value of each variable according to the dominant modality.

760

761 *PPC inactivation by muscimol injection*

762 After the mice became proficient in performing audiovisual discrimination task, we
763 made craniotomies (diameter ~0.5 mm) on both left and right PPC a day before starting
764 sequential multisensory tests. Except for the injection times, we covered the surface of the
765 craniotomies by applying Dura-Gel (Cambridge NeuroTech) not to damage the cortex. We
766 conducted the sequential multisensory tests as follows: Day 1, test without any injection. Day
767 2, rest. Day 3, test with muscimol (Sigma-Aldrich) injection. Day 4, rest. Day 5, test with PBS
768 injection. Day 6, rest. Day 7, test with fluorophore-conjugated muscimol (FCM, Invitrogen)
769 injection. We injected muscimol (1 μg/μl; 40 nl in 2 mice or 60nl in 4 mice), PBS (1X; same
770 volume as the muscimol), or 200 nl of FCM into the PPC at both hemispheres (depth 0.35mm)
771 of the head-fixed awake mice at a speed of 1nl/sec. We started the multisensory test 15 minutes
772 after the end of the injection. We ended the behavioral test at the 320th trials (~45 minutes after
773 the end of the injection) to prevent the effect of overspreading.

774

775 *Optogenetic manipulation*

776 To activate the PV^+ neurons in the right PPC (Fig. 2d-2j), we delivered a continuous
777 blue light from the laser (1 mW or 5 mW at the fiber tip, 473 nm, Shanghai Laser & Optics
778 Century) starting 200 ms before the stimulus presentation (-0.2 ~ 1 s from the stimulus onset)
779 in 50% of trials. To inhibit AC_{PPC} neurons in the right AC or AC_{STR} neurons in the bilateral
780 AC (Fig. 6), we delivered a continuous green light from the laser (5 mW, 532 nm, Shanghai
781 Laser & Optics Century) starting 200ms before the stimulus presentation (-0.2 ~ 1 s from
782 stimulus onset) in 50% of trials. To suppress $M2_{\rightarrow AC}$ axon terminals in the right AC, we
783 delivered a continuous green light from the laser (5 ~ 8 mW, 532 nm) starting 200 ms before
784 the stimulus presentation (-0.2 ~ 1 s from stimulus onset) in 50% of trials. To control the

785 effectiveness of laser light itself during optogenetic inhibition of the target neurons, we
786 conducted control experiments delivering laser lights onto the dental cement.
787

788 **Video monitoring of orofacial and body movements of mice performing a task**

789 The data acquisition and analysis were performed as previously reported[86]. We used a
790 camera (G3-GM11-M2020-Genie, Teledyne DALSA) and lens (TEC-M55 2/3" 55mm
791 telecentric lens, C-Mount) to record left eye of task-performing animals at a high resolution
792 (1200 x 800 pixels) by illuminating the left side of the animal's face with an infrared light
793 source (850 nm, S-IR5850, Skycares). We recorded images at 30 Hz using the Image
794 Acquisition Toolbox provided by MATLAB.

795 We calculated the pupil size of the left eye of the task-performing mice using the
796 following custom-written MATLAB code: 1) drawing an ROI that covers the left eye, 2) setting
797 the optimal brightness threshold to determine the pupil boundary, 3) converting the ROI image
798 to a binary image by filling in each pixel with the black and white values according to the
799 threshold (*imbinarize*, built-in MATLAB function), 4) filling holes within the pupil boundary
800 to avoid any artifacts from measuring pupil area due to light reflection on the cornea (*imfill*,
801 built-in MATLAB function), 5) identifying a convex hull that includes the inside part of the
802 pupil (*bwconvhull*, a built-in MATLAB function), and 6) counting the number of pixels within
803 the convex hull as the pupil size across frames. We normalized the pupil size using the
804 following equation, resulting in a number ranging from 0 (smallest size) to 1 (largest size):

805 $$(10) \quad Normalized\ Pupil(t) = \frac{Pupil(t) - \min(Pupil)}{\max(Pupil)}$$

806

807 ***In vivo* calcium imaging experiments with miniature microscope**

808 *Data acquisition*

809 To avoid bleaching of calcium signals during the behavior task, we conducted an
810 imaging experiment in a stationary or moving block one day and tested the other block the next
811 day. Each imaging session was completed when mice showed three consecutive miss trials or
812 when the imaging time reached one hour. We analyzed the same neurons tracked over two
813 consecutive days in imaging data.

814 We performed an *in vivo* calcium imaging experiment using a miniature fluorescence
815 microscope (Inscopix). Images were acquired at 20 frames per second (10 for AC_{PPC} neurons)
816 using nVista HD software (Inscopix). We cropped superfluous imaging areas that contained no
817 neural signal. The LED power (0.2 ~ 0.5 mW) and gain value (1 ~ 4) were adjusted based on
818 the overall brightness of the GCaMP signals. For the simultaneous *in vivo* calcium imaging
819 with optogenetic axon manipulations (Fig. 7 and Fig. 8c and 8d), we used the nVoke system
820 (Inscopix) to acquire images at 10 frames per second with 0.4 mW of red EX-LED light for
821 optogenetic manipulation on ChrimsonR or eNpHR3.0 expressed in axons. The light delivery
822 started 200ms before the stimulus onset and ended at the stimulation offset (-0.2 ~ 1 s from the
823 stimulus onset).

824

825 *Preprocessing of imaging data*

826 The acquired image data were processed with Inscopix Data Processing Software
827 (IDPS, Inscopix). Images were downsampled by a factor of 4 and spatially filtered (highCutoff:
828 0.5; lowCutoff: 0.01 for PPC excitatory neurons; highCutoff: 0.5; lowCutoff: 0.005 for the
829 other groups). Filtered images were corrected for lateral motion (IDPS implementation).
830 Motion-corrected images were converted to ΔF/F images where F represents the average
831 intensity of each pixel during the whole imaging time. Principal component analysis -
832 independent component analysis (PCA-ICA) was used to identify cell boundaries on ΔF/F
833 images using IDPS implementation. We next extracted calcium signals by manually inspecting

834 cell boundaries obtained from PCA-ICA on motion-corrected images and exported average
835 intensities within cell boundaries. The same neurons were identified throughout several
836 imaging sessions using longitudinal registration (IDPS implementation), and only neurons that
837 appeared across imaging sessions were selected for further analysis.
838
839 *Calculation of response amplitudes, neuronal type classification, and stimulus selectivity*
840 Exported calcium data were analyzed using custom MATLAB codes. The extracted
841 calcium response data was converted to ΔF/F for each neuron. ΔF/F was calculated as
842 $$(11) \quad \Delta F/F = (F - F0)/F0$$
843 , where F0 represents the average fluorescence of a neuron across the imaging time. All the
844 analyses were conducted based on the ΔF/F value.
845 To determine if a neuron responded to distinct stimuli (Fig. 3c), we compared average
846 calcium activity during baseline (-0.2 ~ 0 s) and stimulation (0 ~ 1 s) periods using Wilcoxon
847 signed-rank test ($P < 0.01$, MATLAB implementation). The response amplitude for each trial
848 was calculated by subtracting the average of baseline activity from the average of calcium
849 activity during the first 1 s after stimulus onset. To dissect neuronal type (Fig. 3c), we compared
850 Go and No-go responses if neurons showed significant responses to Go and No-go stimuli in
851 one modality and classified as Go or No-go neurons if they had a significantly stronger
852 response in the Go or No-go trials. Neurons that showed significant responses in one auditory
853 and one visual stimulus were classified as "Dual," while neurons with significant responses in
854 three unisensory trial types were classified as "Triple." "All" type neurons responded
855 significantly in all unisensory trials. To examine how locomotion affects unisensory responses
856 (Supplementary Fig. 2a), we compared the response amplitudes of each neuron from stationary
857 and moving sessions using the Mann-Whitney U-test ($P < 0.01$).

To calculate the change in spontaneous activity of imaged neurons by locomotion onset and offset, we collected calcium activity and locomotion speed data at all locomotion onsets or offsets (-2 ~ 2 s) and concatenated them. We then calculated the Pearson correlation coefficient between the two variables. We used the following conditions to define locomotion onset and offset during an imaging session.

Locomotion onset at 0 s must satisfy all of the following conditions:

1) *Average locomotion speed (-1 ~ -0.5 s) < 0.5cm/s;*

2) *Average locomotion speed (-0.5 ~ 0 s) < 0.5cm/s;*

3) Average locomotion speed (0 ~ 250 ms) > 1cm/s;

4) Average locomotion speed (250 ~ 1000 ms) > 2cm/s;

5) No stimulus during -2 ~ 2 s.

Locomotion offset at 0 s must satisfy all of the following conditions:

1) *Average locomotion speed (-1 ~ -0.5 s) > 2 cm/s;*

2) *Average locomotion speed (-0.5 ~ 0 s) > 1cm/s;*

3) Average locomotion speed (0 ~ 250 ms) < 0.5cm/s;

4) Average locomotion speed (250 ~ 1000 ms) < 0.5cm/s;

5) No stimulus during -2 ~ 2 s.

To calculate the change in $M2_{AC}$ activity at locomotion onset (Fig. 8i), we subtracted mean baseline activity (-1 ~ -0.5 s from locomotion onset) from mean calcium signal at early (0 ~ 1.5 s from locomotion onset) or late (3 s from locomotion onset ~ -1 s from locomotion offset) periods.

To compare the stimulus selectivity (Supplementary Fig. 5), we excluded neurons that were not responsive to the stimulus in either stationary or moving states. We calculated the stimulus selectivity of each neuron as the following formula.

882 (12) $$Selectivity\ index = \frac{|Average\ amplitude(stim\ A)| - |Average\ amplitude(stim\ B)|}{|Average\ amplitude(stim\ A)| + |Average\ amplitude(stim\ B)|}$$

883

884 *Demixed principal component analysis of imaging data*

885 To visualize populational activity during the behavioral task over time, we used
886 demixed principal component analysis (dPCA)[72]. The dPCA was performed using trial-
887 averaged calcium activity aligned at stimulus onset (-1 ~ 3 s) of all neurons across the eight
888 unisensory trial types (visual hit, visual miss, visual CR, visual FA, auditory hit, auditory miss,
889 auditory CR, and auditory FA). To denoise the calcium data, we temporally downsampled it
890 (factor 2) and applied Gaussian smoothing with a window size of three bins. We excluded
891 sessions that had fewer than three trials of lick or no-lick in unisensory and incongruent trials.
892 The encoding PCs from the dPCA were classified into stimulus-related, decision-related,
893 stimulus-decision interaction-related, and independent axes. To show trajectories for each trial
894 type in Fig. 3g, 4a, 4c, and Supplementary Fig. 6d,7d, we used dPCA results derived from all
895 imaged neurons. For all quantifications, we used the dPCA results from each imaging session.
896 We projected the activities of multisensory trials (congruent and incongruent trials) by using
897 transformation vectors obtained from the dPCA with the unisensory trials.

898 To quantify the similarities between trial types, we calculated Euclidean distances
899 between coordinates after the stimulus onset (0 ~ 1 s) in a subspace containing the top 3
900 stimulus PCs. To compare neural trajectories based on locomotion state, trial-averaged
901 activities of unisensory trials from stationary, start-moving, and keep-moving trials were
902 analyzed by dPCA. To distinguish between start-moving and keep-moving data in the moving
903 sessions, we projected trial data into the encoding PC axes from the dPCA of each moving
904 session. The Euclidean distance between two trajectories was calculated 1 s after the stimulus

905 onset. Projection distance was measured as the Euclidean distance between 0 and 1 s following
906 the stimulus onset.
907
908 *dPCA based classifiers*
909 For classifiers (Fig. 3 and Supplementary Fig. 3,6,7), we projected single-trial activity
910 onto the top encoding PC axes and computed Euclidean distances between single trial data
911 (only correct trials for unisensory classification) and trial-averaged trajectories of unisensory
912 trials (for unisensory classification) or incongruent trials (for incongruent classification) at each
913 time points. Each test trial was classified into a trial type of trial-averaged trajectory that
914 showed the smallest Euclidean distance from the test trial trajectory. If the test trajectory
915 showed a very short projection on the PC axes, its distance to the center of the pre-stimulus
916 trajectories was smaller than its distance to the trial-averaged trajectories at each time point.
917 We counted such trials as incorrect classification.
918 To determine the significance of similarity with visual trajectories in determining
919 dominant modality (Fig. 4e,f), we first projected the activities of individual unisensory trials
920 onto the top three stimulus encoding PC axes and calculated the Euclidean distance between
921 each trajectory and the trial-averaged target visual trajectory (target visual trajectory: V_G for
922 $A_{NG}V_G$ classification; V_{NG} for A_GV_{NG} classification). To calculate the distribution of individual
923 visual trials, we used linear discriminant analysis (LDA) to determine an Euclidean distance
924 threshold that distinguishes visual trials from other visual and auditory trials. Finally, we
925 classified individual incongruent trials according to their Euclidean distance to the trial-
926 averaged target visual trajectory, with each trial classified as a visual-dominant trial if its
927 Euclidean distance was less than the threshold. To statistically compare classifier accuracies,
928 we calculated mean classifier accuracy between 0.5 and 1 s following stimulus onset, when the
929 classifiers attained a peak of classification accuracy, and compared between groups.

930

931 ***In vivo* calcium imaging experiments with 2-photon microscope**

932 *Data acquisition*

933 We performed an *in vivo* calcium imaging experiment using a 2-photon microscope
934 (BergamoII, Thorlabs). We adjusted the wavelength of the tuneable excitatory laser (InsightX3,
935 Spectra-Physics) to 920 nm for imaging green channels and 1040 nm for imaging red channels.
936 The laser power was calibrated as 60~80 mW at the position of the focal plane from the
937 objective lens (XLUMPLFLN20XW, Olympus). We used an ultrasonic clear gel as the
938 immersion medium and covered the gap between the mouse's head and the objective lens with
939 a fabric curtain to prevent light from the stimulus monitor from being detected. To increase the
940 number of neurons imaged in each session, we conducted three-plane imaging with 30 μm
941 intervals, capturing 7.4 images/s in each plane. The image size was 512 × 512 pixels,
942 corresponding to an actual imaging field size of 600 × 600 μm (imaging center: posterior 3.5
943 mm and lateral 2.5mm from the bregma). For the red channel imaging to identify VC_{PPC}
944 neurons in each imaging field, we collected images for 1 minute from the same planes we
945 conducted calcium imaging.

946

947 *Processing of imaging data*

948 We used Suite2p for motion correction and cell detection for our 2-photon imaging
949 data[87]. For a brief explanation, we conducted non-rigid motion correction (Suite2p
950 implementation) and used extracted fluorescent signals of soma and neuropil. After cell
951 identification, we manually sorted good cells in each field of view. For the neuropil correction,
952 the corrected fluorescence value for each cell was calculated as follows.

953 $$F_{corrected}(t) = F_{soma}(t) - 0.7 \times F_{neuropil}(t) \quad (13)$$

954 The baseline for ΔF/F calculation was the 10th percentile of $F_{corrected}$ within a sliding window
955 of 3 mins duration. The rest of the analysis was conducted in the same methods as the data
956 analysis of miniature microscope imaging data. To identify VC_{PPC} neurons in each imaging
957 field, we overlapped the representative red image made by motion correction followed by z-
958 projection to the Suite2p result and manually identified them.
959
960 **Histology and Immunohistochemistry**
961 We performed histology experiments to confirm imaging sites after *in vivo* calcium imaging,
962 injection and expression sites of viral vectors, and anatomical circuit tracing data. Mice were
963 anesthetized with avertin (2,2,2-Tribromoethanol (Sigma-Aldrich), 125-250mg/kg,
964 intraperitoneally) and transcardially perfused with 15ml of PBS, followed by 4%
965 paraformaldehyde (PFA, w/v in PBS). Brain samples were post-fixed for 4 hours in the PFA
966 at 4°C, then washed 3 times with PBS for 10 minutes each. After washing, the brain samples
967 were immersed in a 30% sucrose solution (w/v in PBS) for 2-5 days. When the brain samples
968 sank, they were embedded in an optimal cutting temperature medium (Tissue-Tek O.C.T.
969 Compound, Sakura Finetek) and rapidly froze at -80°C. Frozen brain samples were sectioned
970 into 40 μm or 20 μm (for immunostaining) in a coronal direction using a cryocut (Leica). We
971 washed brain slices 3 times in PBS for 10 minutes before mounting them with an anti-bleaching
972 mounting medium containing 4′,6-diamidino-2-phenylindole (DAPI) (Vector Labs). To
973 immunostain the CaMKIIα or PV, we permeabilized the brain sections for 30 min with 0.5%
974 w/v Triton X-100 in PBS, then blocked with 2% w/v normal goat serum (NGS) in PBS for 2
975 hours at room temperature. The samples were incubated at 4°C for 48 hours with mouse anti-
976 CaMKIIα antibodies (ab22609, abcam, 1:250 dilution in 2% NGS) or rabbit anti-PV antibodies
977 (PV27, swant, 1:500 dilution in 2% NGS). After treating the primary antibodies, we washed
978 the samples 3 times in PBS for 10 minutes. We used Alexa Fluor 594 goat anti-mouse IgG

979 (A11005, Invitrogen, 1:250 dilution in PBS) to stain CaMKIIα or Alexa Fluor 594 goat anti-
980 rabbit IgG (A21207, Invitrogen, 1:500 dilution in PBS) to stain PV for 2 hours at room
981 temperature. Following that, we washed the samples in PBS 3 times for 10 minutes before
982 mounting them with an anti-bleaching medium with DAPI. Fluorescent images of brain slices
983 were taken using a slide scanner (Zeiss Axio Scan. Z1) or a confocal microscope (Nikon A1
984 HD25).
985

986 **Statistical analysis**

987 We analyzed the data using custom-written codes in MATLAB (Mathworks). All data were
988 presented as mean ± SEM unless otherwise noted. 'N' denotes the number of mice or sessions,
989 whereas 'n' represents the number of neurons. All statistical analyses were described in the
990 figure legends. We first tested the normality of the data using the Shapiro-Wilk test and applied
991 parametric or non-parametric statistical analyses accordingly. For multiple comparisons, we
992 performed Bonferroni correction on the statistical results or used ANOVA for data that passed
993 the normality test to avoid the increased probability of Type II errors associated with
994 Bonferroni correction when analyzing a high number of pairs (> 6 pairs). All the statistical
995 significances of the datasets were indicated as NS (not significant; $P \geq 0.1$), # ($P < 0.1$), * ($P < 0.05$), ** ($P < 0.01$), *** ($P < 0.001$), and **** ($P < 0.0001$).

Data availability

Source data are provided with this paper. All the representative data that support the findings are publicly available on GitHub: https://github.com/seungheelee1789/PPC_Choi. Further requests for the data generated in this study can be directed to the corresponding author (shlee1@kaist.ac.kr).

Code availability

All the custom MATLAB codes to analyze and visualize the data are publicly available on GitHub (https://github.com/seungheelee1789/PPC_Choi).

References

1 Stein, B. E. *The new handbook of multisensory processing*. (MIT Press, 2012).

2 Gielen, S. C., Schmidt, R. A. & Van den Heuvel, P. J. On the nature of intersensory facilitation of reaction time. *Percept Psychophys* **34**, 161-168 (1983). https://doi.org/10.3758/bf03211343

3 Diederich, A. & Colonius, H. Bimodal and trimodal multisensory enhancement: effects of stimulus onset and intensity on reaction time. *Percept Psychophys* **66**, 1388-1404 (2004). https://doi.org/10.3758/bf03195006

4 Raposo, D., Sheppard, J. P., Schrater, P. R. & Churchland, A. K. Multisensory decision-making in rats and humans. *J Neurosci* **32**, 3726-3735 (2012). https://doi.org/10.1523/JNEUROSCI.4998-11.2012

5 Meijer, G. T., Pie, J. L., Dolman, T. L., Pennartz, C. M. A. & Lansink, C. S. Audiovisual Integration Enhances Stimulus Detection Performance in Mice. *Front Behav Neurosci* **12**, 231 (2018). https://doi.org/10.3389/fnbeh.2018.00231

6 Colavita, F. B. Human Sensory Dominance. *Perception & Psychophysics* **16**, 409-412 (1974). https://doi.org/Doi 10.3758/Bf03203962

7 McGurk, H. & MacDonald, J. Hearing lips and seeing voices. *Nature* **264**, 746-748 (1976). https://doi.org/10.1038/264746a0

8 Battaglia, P. W., Jacobs, R. A. & Aslin, R. N. Bayesian integration of visual and auditory signals for spatial localization. *J Opt Soc Am A Opt Image Sci Vis* **20**, 1391-1397 (2003). https://doi.org/10.1364/josaa.20.001391

9 Alais, D. & Burr, D. The ventriloquist effect results from near-optimal bimodal integration. *Curr Biol* **14**, 257-262 (2004). https://doi.org/10.1016/j.cub.2004.01.029

10 Fetsch, C. R., Turner, A. H., DeAngelis, G. C. & Angelaki, D. E. Dynamic reweighting of visual and vestibular cues during self-motion perception. *J Neurosci* **29**, 15601-15612 (2009). https://doi.org/10.1523/JNEUROSCI.2574-09.2009

11 Fetsch, C. R., Pouget, A., DeAngelis, G. C. & Angelaki, D. E. Neural correlates of reliability-based cue weighting during multisensory integration. *Nat Neurosci* **15**, 146-154 (2011). https://doi.org/10.1038/nn.2983

12 Song, Y. H. *et al.* A Neural Circuit for Auditory Dominance over Visual Perception. *Neuron* **93**, 940-+ (2017). https://doi.org/10.1016/j.neuron.2017.01.006

13 Choi, I. & Lee, S. H. Reduced activity of parvalbumin-positive interneurons in the posterior parietal cortex causes visually dominant multisensory decisions in freely

navigating mice. *Mol Brain* **15**, 82 (2022). https://doi.org/10.1186/s13041-022-00968-x

14 Ernst, M. O. & Banks, M. S. Humans integrate visual and haptic information in a statistically optimal fashion. *Nature* **415**, 429-433 (2002). https://doi.org/10.1038/415429a

15 Kording, K. P. & Wolpert, D. M. Bayesian integration in sensorimotor learning. *Nature* **427**, 244-247 (2004). https://doi.org/10.1038/nature02169

16 Coen, P., Sit, T. P. H., Wells, M. J., Carandini, M. & Harris, K. D. Mouse frontal cortex mediates additive multisensory decisions. *Neuron* **111**, 2432-2447 e2413 (2023). https://doi.org/10.1016/j.neuron.2023.05.008

17 Keil, J., Muller, N., Ihssen, N. & Weisz, N. On the variability of the McGurk effect: audiovisual integration depends on prestimulus brain states. *Cereb Cortex* **22**, 221-231 (2012). https://doi.org/10.1093/cercor/bhr125

18 Jiang, W., Jiang, H. & Stein, B. E. Two corticotectal areas facilitate multisensory orientation behavior. *J Cogn Neurosci* **14**, 1240-1255 (2002). https://doi.org/10.1162/089892902760807230

19 Avillac, M., Ben Hamed, S. & Duhamel, J. R. Multisensory integration in the ventral intraparietal area of the macaque monkey. *J Neurosci* **27**, 1922-1932 (2007). https://doi.org/10.1523/JNEUROSCI.2646-06.2007

20 Mallick, D. B., Magnotti, J. F. & Beauchamp, M. S. Variability and stability in the McGurk effect: contributions of participants, stimuli, time, and response type. *Psychon Bull Rev* **22**, 1299-1307 (2015). https://doi.org/10.3758/s13423-015-0817-4

21 Sinnett, S., Spence, C. & Soto-Faraco, S. Visual dominance and attention: the Colavita effect revisited. *Percept Psychophys* **69**, 673-686 (2007). https://doi.org/10.3758/bf03193770

22 Crochet, S., Lee, S. H. & Petersen, C. C. H. Neural Circuits for Goal-Directed Sensorimotor Transformations. *Trends Neurosci* **42**, 66-77 (2019). https://doi.org/10.1016/j.tins.2018.08.011

23 Esmaeili, V. *et al.* Rapid suppression and sustained activation of distinct cortical regions for a delayed sensory-triggered motor response. *Neuron* **109**, 2183-2201 e2189 (2021). https://doi.org/10.1016/j.neuron.2021.05.005

1070 24 Choi, I., Lee, J. Y. & Lee, S. H. Bottom-up and top-down modulation of multisensory
1071 integration. *Curr Opin Neurobiol* **52**, 115-122 (2018).
1072 https://doi.org/10.1016/j.conb.2018.05.002
1073 25 McGinley, M. J. *et al.* Waking State: Rapid Variations Modulate Neural and Behavioral
1074 Responses. *Neuron* **87**, 1143-1161 (2015).
1075 https://doi.org/10.1016/j.neuron.2015.09.012
1076 26 Ayaz, A., Saleem, A. B., Scholvinck, M. L. & Carandini, M. Locomotion controls
1077 spatial integration in mouse visual cortex. *Curr Biol* **23**, 890-894 (2013).
1078 https://doi.org/10.1016/j.cub.2013.04.012
1079 27 Bennett, C., Arroyo, S. & Hestrin, S. Subthreshold Mechanisms Underlying State-
1080 Dependent Modulation of Visual Responses. *Neuron* **80**, 350-357 (2013).
1081 https://doi.org/10.1016/j.neuron.2013.08.007
1082 28 Dipoppa, M. *et al.* Vision and Locomotion Shape the Interactions between Neuron
1083 Types in Mouse Visual Cortex. *Neuron* **98**, 602-+ (2018).
1084 https://doi.org/10.1016/j.neuron.2018.03.037
1085 29 Fu, Y. *et al.* A Cortical Circuit for Gain Control by Behavioral State. *Cell* **156**, 1139-
1086 1152 (2014). https://doi.org/10.1016/j.cell.2014.01.050
1087 30 Lee, A. M. *et al.* Identification of a Brainstem Circuit Regulating Visual Cortical State
1088 in Parallel with Locomotion. *Neuron* **83**, 455-466 (2014).
1089 https://doi.org/10.1016/j.neuron.2014.06.031
1090 31 Niell, C. M. & Stryker, M. P. Modulation of Visual Responses by Behavioral State in
1091 Mouse Visual Cortex. *Neuron* **65**, 472-479 (2010).
1092 https://doi.org/10.1016/j.neuron.2010.01.033
1093 32 Paken, J. M. P. *et al.* Behavioral-state modulation of inhibition is context-dependent
1094 and cell type specific in mouse visual cortex. *Elife* **5** (2016). https://doi.org/ARTN
1095 e14985
1096 10.7554/eLife.14985
1097 33 Polack, P. O., Friedman, J. & Golshani, P. Cellular mechanisms of brain state-
1098 dependent gain modulation in visual cortex. *Nature Neuroscience* **16**, 1331-U1227
1099 (2013). https://doi.org/10.1038/nn.3464
1100 34 Vinck, M., Batista-Brito, R., Knoblich, U. & Cardin, J. A. Arousal and Locomotion
1101 Make Distinct Contributions to Cortical Activity Patterns and Visual Encoding. *Neuron*
1102 **86**, 740-754 (2015). https://doi.org/10.1016/j.neuron.2015.03.028

35 McGinley, M. J., David, S. V. & McCormick, D. A. Cortical Membrane Potential Signature of Optimal States for Sensory Signal Detection. *Neuron* **87**, 179-192 (2015). https://doi.org/10.1016/j.neuron.2015.05.038

36 Zhou, M. *et al.* Scaling down of balanced excitation and inhibition by active behavioral states in auditory cortex. *Nature Neuroscience* **17**, 841-850 (2014). https://doi.org/10.1038/nn.3701

37 Nelson, A. *et al.* A Circuit for Motor Cortical Modulation of Auditory Cortical Activity. *Journal of Neuroscience* **33**, 14342-+ (2013). https://doi.org/10.1523/Jneurosci.2275-13.2013

38 Schneider, D. M., Nelson, A. & Mooney, R. A synaptic and circuit basis for corollary discharge in the auditory cortex. *Nature* **513**, 189-+ (2014). https://doi.org/10.1038/nature13724

39 Schneider, D. M., Sundararajan, J. & Mooney, R. A cortical filter that learns to suppress the acoustic consequences of movement. *Nature* **561**, 391-+ (2018). https://doi.org/10.1038/s41586-018-0520-5

40 Runyan, C. A., Piasini, E., Panzeri, S. & Harvey, C. D. Distinct timescales of population coding across cortex. *Nature* **548**, 92-96 (2017). https://doi.org/10.1038/nature23020

41 Williamson, R. S., Hancock, K. E., Shinn-Cunningham, B. G. & Polley, D. B. Locomotion and Task Demands Differentially Modulate Thalamic Audiovisual Processing during Active Search. *Curr Biol* **25**, 1885-1891 (2015). https://doi.org/10.1016/j.cub.2015.05.045

42 Zhou, Y. & Freedman, D. J. Posterior parietal cortex plays a causal role in perceptual and categorical decisions. *Science* **365**, 180-185 (2019). https://doi.org/10.1126/science.aaw8347

43 Lyamzin, D. & Benucci, A. The mouse posterior parietal cortex: Anatomy and functions. *Neurosci Res* **140**, 14-22 (2019). https://doi.org/10.1016/j.neures.2018.10.008

44 Freedman, D. J. & Ibos, G. An Integrative Framework for Sensory, Motor, and Cognitive Functions of the Posterior Parietal Cortex. *Neuron* **97**, 1219-1234 (2018). https://doi.org/10.1016/j.neuron.2018.01.044

45 Goard, M. J., Pho, G. N., Woodson, J. & Sur, M. Distinct roles of visual, parietal, and frontal motor cortices in memory-guided sensorimotor decisions. *Elife* **5** (2016). https://doi.org/10.7554/eLife.13764

46 Nikbakht, N., Tafreshiha, A., Zoccolan, D. & Diamond, M. E. Supralinear and Supramodal Integration of Visual and Tactile Signals in Rats: Psychophysics and Neuronal Mechanisms. *Neuron* **97**, 626-639 e628 (2018). https://doi.org/10.1016/j.neuron.2018.01.003

47 Oude Lohuis, M. N., Marchesi, P., Pennartz, C. M. A. & Olcese, U. Functional (ir)relevance of posterior parietal cortex during audiovisual change detection. *J Neurosci* **42**, 5229-5245 (2022). https://doi.org/10.1523/JNEUROSCI.2150-21.2022

48 Licata, A. M. *et al.* Posterior Parietal Cortex Guides Visual Decisions in Rats. *J Neurosci* **37**, 4954-4966 (2017). https://doi.org/10.1523/JNEUROSCI.0105-17.2017

49 Morcos, A. S. & Harvey, C. D. History-dependent variability in population dynamics during evidence accumulation in cortex. *Nat Neurosci* **19**, 1672-1681 (2016). https://doi.org/10.1038/nn.4403

50 Scott, B. B. *et al.* Fronto-parietal Cortical Circuits Encode Accumulated Evidence with a Diversity of Timescales. *Neuron* **95**, 385-398 e385 (2017). https://doi.org/10.1016/j.neuron.2017.06.013

51 Hwang, E. J., Dahlen, J. E., Mukundan, M. & Komiyama, T. History-based action selection bias in posterior parietal cortex. *Nat Commun* **8**, 1242 (2017). https://doi.org/10.1038/s41467-017-01356-z

52 Driscoll, L. N., Pettit, N. L., Minderer, M., Chettih, S. N. & Harvey, C. D. Dynamic Reorganization of Neuronal Activity Patterns in Parietal Cortex. *Cell* **170**, 986-999 e916 (2017). https://doi.org/10.1016/j.cell.2017.07.021

53 Harvey, C. D., Coen, P. & Tank, D. W. Choice-specific sequences in parietal cortex during a virtual-navigation decision task. *Nature* **484**, 62-68 (2012). https://doi.org/10.1038/nature10918

54 Pho, G. N., Goard, M. J., Woodson, J., Crawford, B. & Sur, M. Task-dependent representations of stimulus and choice in mouse parietal cortex. *Nat Commun* **9**, 2596 (2018). https://doi.org/10.1038/s41467-018-05012-y

55 Tseng, S. Y., Chettih, S. N., Arlt, C., Barroso-Luque, R. & Harvey, C. D. Shared and specialized coding across posterior cortical areas for dynamic navigation decisions. *Neuron* **110**, 2484-2502 e2416 (2022). https://doi.org/10.1016/j.neuron.2022.05.012

56 Raposo, D., Kaufman, M. T. & Churchland, A. K. A category-free neural population supports evolving demands during decision-making. *Nature Neuroscience* **17**, 1784-1792 (2014). https://doi.org/10.1038/nn.3865

57 Akrami, A., Kopec, C. D., Diamond, M. E. & Brody, C. D. Posterior parietal cortex represents sensory history and mediates its effects on behaviour. *Nature* **554**, 368-372 (2018). https://doi.org/10.1038/nature25510

58 Zhong, L. *et al.* Causal contributions of parietal cortex to perceptual decision-making during stimulus categorization. *Nat Neurosci* **22**, 963-973 (2019). https://doi.org/10.1038/s41593-019-0383-6

59 Hanks, T. D. *et al.* Distinct relationships of parietal and prefrontal cortices to evidence accumulation. *Nature* **520**, 220-223 (2015). https://doi.org/10.1038/nature14066

60 Erlich, J. C., Brunton, B. W., Duan, C. A., Hanks, T. D. & Brody, C. D. Distinct effects of prefrontal and parietal cortex inactivations on an accumulation of evidence task in the rat. *Elife* **4** (2015). https://doi.org/10.7554/eLife.05457

61 Gallero-Salas, Y. *et al.* Sensory and Behavioral Components of Neocortical Signal Flow in Discrimination Tasks with Short-Term Memory. *Neuron* **109**, 135-148 e136 (2021). https://doi.org/10.1016/j.neuron.2020.10.017

62 Yao, J. D., Gimoto, J., Constantinople, C. M. & Sanes, D. H. Parietal Cortex Is Required for the Integration of Acoustic Evidence. *Curr Biol* **30**, 3293-3303 e3294 (2020). https://doi.org/10.1016/j.cub.2020.06.017

63 Zingg, B. *et al.* Neural networks of the mouse neocortex. *Cell* **156**, 1096-1111 (2014). https://doi.org/10.1016/j.cell.2014.02.023

64 Zhang, S. *et al.* Organization of long-range inputs and outputs of frontal cortex for top-down control. *Nat Neurosci* **19**, 1733-1742 (2016). https://doi.org/10.1038/nn.4417

65 Lewis, J. W. & Van Essen, D. C. Corticocortical connections of visual, sensorimotor, and multimodal processing areas in the parietal lobe of the macaque monkey. *J Comp Neurol* **428**, 112-137 (2000). https://doi.org/10.1002/1096-9861(20001204)428:1<112::aid-cne8>3.0.co;2-9

66 Driver, J. & Noesselt, T. Multisensory interplay reveals crossmodal influences on 'sensory-specific' brain regions, neural responses, and judgments. *Neuron* **57**, 11-23 (2008). https://doi.org/10.1016/j.neuron.2007.12.013

67 Schlack, A., Sterbing-D'Angelo, S. J., Hartung, K., Hoffmann, K. P. & Bremmer, F. Multisensory space representations in the macaque ventral intraparietal area. *J Neurosci* **25**, 4616-4625 (2005). https://doi.org/10.1523/JNEUROSCI.0455-05.2005

68 Olcese, U., Iurilli, G. & Medini, P. Cellular and synaptic architecture of multisensory integration in the mouse neocortex. *Neuron* **79**, 579-593 (2013). https://doi.org/10.1016/j.neuron.2013.06.010

69 Wallace, M. T., Ramachandran, R. & Stein, B. E. A revised view of sensory cortical parcellation. *Proc Natl Acad Sci U S A* **101**, 2167-2172 (2004). https://doi.org/10.1073/pnas.0305697101

70 Shimaoka, D., Harris, K. D. & Carandini, M. Effects of Arousal on Mouse Sensory Cortex Depend on Modality (vol 22, pg 3160, 2018). *Cell Reports* **25**, 3230-3230 (2018). https://doi.org/10.1016/j.celrep.2018.11.105

71 Schneider, D. M. & Mooney, R. Motor-related signals in the auditory system for listening and learning. *Curr Opin Neurobiol* **33**, 78-84 (2015). https://doi.org/10.1016/j.conb.2015.03.004

72 Kobak, D. *et al.* Demixed principal component analysis of neural population data. *Elife* **5** (2016). https://doi.org/10.7554/eLife.10989

73 Chen, L., Wang, X. X., Ge, S. Y. & Xiong, Q. J. Medial geniculate body and primary auditory cortex differentially contribute to striatal sound representations. *Nature Communications* **10** (2019). https://doi.org/ARTN 418
10.1038/s41467-019-08350-7

74 Guo, L., Walker, W. I., Ponvert, N. D., Penix, P. L. & Jaramillo, S. Stable representation of sounds in the posterior striatum during flexible auditory decisions. *Nature Communications* **9** (2018). https://doi.org/ARTN 1534
10.1038/s41467-018-03994-3

75 Xiong, Q. J., Znamenskiy, P. & Zador, A. M. Selective corticostriatal plasticity during acquisition of an auditory discrimination task. *Nature* **521**, 348-+ (2015). https://doi.org/10.1038/nature14225

76 Ponvert, N. D. & Jaramillo, S. Auditory Thalamostriatal and Corticostriatal Pathways Convey Complementary Information about Sound Features. *Journal of Neuroscience* **39**, 271-280 (2019). https://doi.org/10.1523/Jneurosci.1188-18.2018

77 Lin, P. A., Asinof, S. K., Edwards, N. J. & Isaacson, J. S. Arousal regulates frequency tuning in primary auditory cortex. *Proc Natl Acad Sci U S A* **116**, 25304-25310 (2019). https://doi.org/10.1073/pnas.1911383116

78 Welch, R. B. & Warren, D. H. Immediate perceptual response to intersensory discrepancy. *Psychol Bull* **88**, 638-667 (1980).

79 Repp, B. H. & Penel, A. Auditory dominance in temporal processing: New evidence from synchronization with simultaneous visual and auditory sequences. *J Exp Psychol Human* **28**, 1085-1099 (2002). https://doi.org/10.1037//0096-1523.28.5.1085

80 Crapse, T. B. & Sommer, M. A. Corollary discharge across the animal kingdom. *Nat Rev Neurosci* **9**, 587-600 (2008). https://doi.org/10.1038/nrn2457

81 Kuan, A. T. *et al.* Synaptic wiring motifs in posterior parietal cortex support decision-making. *bioRxiv*, 2022.2004.2013.488176 (2022). https://doi.org/10.1101/2022.04.13.488176

82 Romanski, L. M. Representation and integration of auditory and visual stimuli in the primate ventral lateral prefrontal cortex. *Cereb Cortex* **17 Suppl 1**, i61-69 (2007). https://doi.org/10.1093/cercor/bhm099

83 Calvert, G. A., Campbell, R. & Brammer, M. J. Evidence from functional magnetic resonance imaging of crossmodal binding in the human heteromodal cortex. *Curr Biol* **10**, 649-657 (2000). https://doi.org/10.1016/s0960-9822(00)00513-3

84 Gulati, S., Cao, V. Y. & Otte, S. Multi-layer Cortical Ca2+ Imaging in Freely Moving Mice with Prism Probes and Miniaturized Fluorescence Microscopy. *Jove-J Vis Exp* (2017). https://doi.org/ARTN e55579
10.3791/55579

85 Goldey, G. J. *et al.* Removable cranial windows for long-term imaging in awake mice. *Nat Protoc* **9**, 2515-2538 (2014). https://doi.org/10.1038/nprot.2014.165

86 Kim, J. H., Ma, D. H., Jung, E., Choi, I. & Lee, S. H. Gated feedforward inhibition in the frontal cortex releases goal-directed action. *Nat Neurosci* **24**, 1452-1464 (2021). https://doi.org/10.1038/s41593-021-00910-9

87 Pachitariu, M. *et al.* Suite2p: beyond 10,000 neurons with standard two-photon microscopy. *bioRxiv*, 061507 (2017). https://doi.org/10.1101/061507

Acknowledgements

We thank Dr. Alex C. Kwan for helpful discussions on imaging data analysis and Dr. Jae-Hyun Kim for assistance with pupil data analysis. This work was supported by grants to S.-H.L. from the National Research Foundation of Korea funded by the Ministry of Science & ICT (NRF-2021R1A2C3012159) and the Institute for Basic Science (IBS-R002-A2).

Author Contributions Statements

I.C. and S.-H.L. conceived and designed all experiments and wrote the manuscript. I.C. performed all experiments and analyzed the data.

Competing Interests Statement

The authors declare no competing interests.

Main figure legends

Fig. 1 | Locomotion shifts auditory-dominant decisions to visually dominant ones in mice under audiovisual conflicts

a, Schematic illustration of the audiovisual discrimination task in a head-fixed mouse on a treadmill. G, go; NG, no-go; L, lick; NL, no lick; FA, false alarm; CR, correct rejection.

b, Stimuli used for behavioral training. Aud, auditory stimuli; Vis, visual stimuli.

c, Learning curves of mice trained on the task. The black dashed line indicates the criterion for expert performance (80% correct rate). Red, visual discrimination performance; Blue, auditory discrimination performance.

d, Schematics of stationary (top, S) and moving (bottom, M) conditions.

e, Audiovisual stimuli used for the multisensory test. Con, congruent stimuli; Incon, incongruent stimuli. Letters 'A' and 'V' after the arrows indicate auditory and visual dominance, respectively.

f, Discriminability (d′) for auditory (Aud), visual (Vis), and congruent (Con) Go/No-go stimuli. Each circle represents one mouse. S, stationary; M, moving.

g, Auditory d′ in mice presented with incongruent (Incon) stimuli. d′ was calculated based on the auditory rules.

h, Auditory dominance rates in incongruent trials across different locomotion states. Auditory dominance rates reflect the fraction of incongruent trials in which mice followed auditory Go/No-go rules. S, stationary; SM, start-moving; KM, keep-moving.

Data are presented as means ± SEM. Thin lines and circles represent individual mouse data. Source data are available in Source Data File. Sample numbers and statistical information are listed in Supplementary Data 1. NS, not significant; ****$P < 0.0001$.

1294 **Fig. 2 | PPC inactivation disrupts visual discrimination and enhances auditory dominance**

1295 **a**, Top, schematic illustration of bilateral muscimol injection into the PPC. Bottom, example
1296 images showing fluorophore-conjugated muscimol (FCM) injected into the PPC. Scale bars:
1297 500μm.

1298 **b**, Changes in d′ (left), hit rates (middle), and FA rates (right) following muscimol injection
1299 compared to PBS injection.

1300 **c**, Multisensory enhancement in congruent trials after muscimol or PBS injections.

1301 **d**, Top, schematic illustration of optogenetic PV^+ activation in the right PPC. Bottom,
1302 fluorescent images showing channelrhodopsin expression in immunostained PV^+ neurons in
1303 the PPC. Scale bars, 20μm.

1304 **e**, Changes in d′ (left), hit rates (middle), and FA rates (right) in PV::ChR2 or PV::eYFP mice
1305 with 1 mW laser stimulation.

1306 **f**, Multisensory enhancement in congruent trials in PV::ChR2 mice with 1 mW laser
1307 stimulation.

1308 **g** and **h**, same as **e** and **f**, but with 5 mW laser stimulation.

1309 **i**, Changes in d′ (left), hit rates (middle), and FA rates (right) with 1 mW or 5 mW laser
1310 stimulation in the same PV::ChR2 mice.

1311 **j**, ΔMultisensory enhancement (laser on – off; 1 mW vs. 5 mW) in congruent trials.

1312 Data are presented as means ± SEM. Circles and gray lines represent individual mouse data.
1313 Source data are available in Source Data File. Sample numbers and statistical information are
1314 listed in Supplementary Data 1. NS, not significant; #$P < 0.1$, *$P < 0.05$, **$P < 0.01$, ***$P <$
1315 0.001, ****$P < 0.0001$.

1316 **Fig. 3 | Locomotion suppresses auditory representation while preserving visual**
1317 **representation in the PPC.**

1318 **a**, Top, schematic of *in vivo* calcium imaging of PPC excitatory neurons in a task-performing
1319 mouse. Bottom left, imaging planes across imaged mice (scale bar: 1mm); bottom right,
1320 immunohistochemical confirmation of CaMKIIα expression in GCaMP6s-expressing neurons
1321 (scale bars: 20 μm).

1322 **b**, Calcium activity from four example neurons (green) and locomotion speed (gray) in a
1323 moving mouse during the task.

1324 **c**, Response types during stationary (left) and moving (right) sessions. Top, percentages of
1325 neurons by response type. Bottom, percentages of unisensory and multisensory neurons.

1326 **d**, Stimulus-evoked amplitudes of PPC excitatory neurons during correct unisensory trials in
1327 stationary vs. moving sessions. Red, visual-selective neurons; blue, auditory-selective neurons;
1328 black, multisensory neurons. Magenta (visual and auditory-selective neurons) and black
1329 (multisensory neurons) cross-lines indicate means ± SD.

1330 **e**, Schematic of dPCA decomposing PPC activity into PC axes representing task-relevant
1331 variables. Stim, stimulus; Deci, decision.

1332 **f**, Explained variances for the top 20 demixed PCs. Asterisks denote statistical comparisons
1333 between stimulus PCs and others.

1334 **g**, Stimulus PC trajectories averaged across unisensory correct trials. Circles mark 1 s after
1335 stimulus onset. Projection distance, Euclidean distance between points at 0 s and 1 s; Go/No-
1336 go distance, Euclidean distance between Go and No-go trajectories at 1 s.

1337 **h**, Projection distances of unisensory trajectories.

1338 **i**, Go/No-go distances in auditory or visual trials.

1339 **j**, Schematic of the dPCA classifier predicting trial types based on Euclidean distances to trial-
1340 averaged trajectories.

k, dPCA classifier accuracy for sorting unisensory trials (left, actual data; right, shuffled trial labels). Solid lines, stationary sessions; dashed lines, moving. For shuffled data, lines represent 95% confidence intervals from 500 repetitions. Colors, unisensory trial types. Magenta, stimulus onset (solid) and offset (dashed).

l, Mean classifier accuracy during 0.5 ~ 1 s post-stimulus period.

Data are presented as mean ± SEM except for **d**. Gray lines represent individual data. Source data are available in Source Data File. Sample numbers and statistical information are listed in Supplementary Data 1. NS, not significant; *$P < 0.05$, **$P < 0.01$, ***$P < 0.001$, ****$P < 0.0001$.

Fig. 4 | Similarity between visual and multisensory representations in the PPC predicts dominant modality in multisensory decisions.

a, Trial-averaged calcium trace trajectories for congruent and unisensory trials in the stimulus subspace during stationary (left) and moving (right) sessions.

b, Euclidean distances between congruent and unisensory trajectories at 1 s after the stimulus onset across locomotion states.

c, Same as **a**, but for incongruent and unisensory trials. Incongruent trajectories resembled visual trajectories when mice made visual-dominant decisions. Black, visual-dominant trials; Gray, auditory-dominant trials. Solid lines, $A_{NG}V_G$ trials; dashed lines, A_GV_{NG} trials.

d, Same as **b**, but between incongruent and unisensory trajectories.

e, Left, example session showing Euclidean distances between individual unisensory trajectories and the trial-averaged V_G trajectory 1 s after stimulus onset. Linear discriminant analysis (LDA) boundaries were set at distances that maximally separated V_G trials from other trials. Right, Euclidean distances between $A_{NG}V_G$ trajectories and the trial-averaged V_G trajectory, using LDA boundaries to classify dominant modalities in $A_{NG}V_G$ trials. Dark gray, visual-dominant trials; light gray, auditory-dominant trials.

f, Left, LDA classifier accuracy in predicting dominance in incongruent trials using actual and shuffled trial labels. Solid lines, $A_{NG}V_G$ trials; Dashed lines, A_GV_{NG} trials. For shuffled data, lines represent 95% confidence interval upper boundaries from 500 repetitions. Magenta, stimulus onset (solid) and offset (dashed). Right, mean classifier accuracies during 0.5 ~ 1 s after stimulus onset.

g, Euclidean distances from incongruent trajectories to visual trajectories and auditory dominance rates at different locomotion states. Left, $A_{NG}V_G$ trials; right, A_GV_{NG} trials. Red crosses, means ± SD.

h, Absolute response amplitudes of visual (top) and auditory (bottom)-responsive neurons during unisensory, congruent, visual-dominant or auditory-dominant incongruent trials at different locomotion states.

Data are presented as means ± SEM except for **g**. Circles and connected lines represent individual data. For box plots, central lines indicate medians; boxes represent the 25th-75th percentiles; whiskers show maximum/minimum values excluding outliers. Source data are available in Source Data File. Sample numbers and statistical information are listed in Supplementary Data 1. NS, not significant; #$P < 0.1$, *$P < 0.05$, **$P < 0.01$, ***$P < 0.001$, ****$P < 0.0001$.

1383 **Fig. 5 | Locomotion preferentially suppresses auditory outputs to the parietal cortex.**

1384 **a**, Schematic illustration (left) and injection sites (right) of retrograde AAVs for dual retrograde
1385 tracing of the AC neurons projecting to the PPC (red, AC_{PPC}) and the posterior STR (green,
1386 AC_{STR}). Scale bars, 1 mm.

1387 **b**, Representative images showing AC_{PPC} and AC_{STR} neurons at the anterior (left, -2.3 mm from
1388 the bregma) and posterior (right, -3.2 mm from the bregma) AC. Tracing experiments were
1389 conducted in 3 mice. White lines, boundaries of the AC; white dashed lines, boundaries
1390 between AC subareas. Scale bars, 500 μm.

1391 **c**, Heatmaps representing percentages of labeled AC_{PPC} neurons (left) or AC_{STR} neurons (right)
1392 in AC subregions at different anterior-posterior coordinates. Gray boxes indicate the anterior
1393 AC (-2.3 ~ -2.5 mm from the bregma).

1394 **d**, Percentages of labeled neurons in the AC. Gray lines represent data from individual brain
1395 samples.

1396 **e**, Schematic illustration of *in vivo* calcium imaging of AC_{PPC} neurons.

1397 **f**, Left, mean calcium traces of AC_{PPC} neurons (green) and mean locomotion speeds of mice
1398 (black) aligned to locomotion onset. Magenta, locomotion onset. Right, distribution of Pearson
1399 correlation coefficients between locomotion speeds and calcium activity of individual neurons
1400 at locomotion onset. The red triangle indicates the mean correlation coefficient across all
1401 neurons. Magenta, zero line.

1402 **g**, Same as **f**, but for locomotion offset. Left, magenta indicates locomotion offset.

1403 **h**, Calcium activity of AC_{PPC} neurons during incongruent trials in the stationary state. Black,
1404 visual-dominant trials; Gray, auditory-dominant trials.

1405 **i**, Same as **h**, but in moving state.

1406 **j**, Mean response amplitudes of AC_{PPC} neurons and auditory dominance rates in $A_{NG}V_{G}$ (left)
1407 and $A_{G}V_{NG}$ (right) trials across locomotion states. Circles connected by gray lines represent
1408 individual mouse data. Red crosses, means ± SD.
1409 **k**-**p**, Same as **e**-**j**, but for AC_{STR} neurons.
1410 Data are presented as means ± SEM except for **j**,**p**. Source data are available in Source Data
1411 File. Sample numbers and statistical information are listed in Supplementary Data 1. NS, not
1412 significant; *$P < 0.05$, **$P < 0.01$, ***$P < 0.001$, ****$P < 0.0001$.

Fig. 6 | Double dissociation of AC_{PPC} and AC_{STR} neurons in perceptual decision-making.

a, Schematic illustration of optogenetic inhibition of AC_{PPC} neurons in stationary mice performing an audiovisual discrimination task.

b, Changes in d′ (left), hit rates (middle), and FA rates (right) following optogenetic inhibition of AC_{PPC} neurons.

c,**d**, Same as **a**,**b**, but for optogenetic inhibition of AC_{STR} neurons.

e, Reduction in auditory dominance following inactivation of AC_{PPC} or AC_{STR} neurons.

f, Correlation between the reductions in auditory discriminability and auditory dominance following inactivation of AC_{STR} neurons. *r*, Pearson correlation coefficient; *p*, significance of the Pearson correlation. Black line, linear regression (slope = 1.37).

Bars, means ± SEM. Gray lines and circles represent individual mouse data. Source data are available in Source Data File. Sample numbers and statistical information are listed in Supplementary Data 1. NS, non-significant; #$P < 0.1$, *$P < 0.05$, **$P < 0.01$, ***$P < 0.001$, ****$P < 0.0001$.

Fig. 7 | Optogenetic inhibition of AC axon terminals reduces auditory-to-visual suppression in the PPC.

a, Schematic illustration of *in vivo* calcium imaging with optogenetic inhibition of AC axon terminals in the PPC.

b, Stimulus-evoked response amplitudes of PPC excitatory neurons in correct unisensory trials across optogenetic LED stimulation states. Red, visual-selective neurons; blue, auditory-selective neurons; gray, multisensory neurons (defined without LED stimulation). Magenta cross-lines, means ± SD for visual- and auditory-selective neurons; black cross-lines, means ± SD for multisensory neurons.

c, Response amplitudes of visual neurons during visual-only, incongruent, and incongruent trials with LED stimulation in the PPC.

d, Changes in d′ (left), hit rates (middle), and FA rates (right) following optogenetic inhibition of AC axon terminals in the PPC. Circles represent individual mouse data.

Bars, means ± SEM. For box plots, central lines indicate medians; boxes represent the 25th-75th percentiles; whiskers show maximum/minimum values excluding outliers. Source data are available in Source Data File. Sample numbers and statistical information are listed in Supplementary Data 1. NS, non-significant; $*P < 0.05$, $**P < 0.01$, $***P < 0.001$, $****P < 0.0001$.

1445 **Fig. 8 | M2-to-AC projection inhibits AC_{PPC} neurons and induces visually dominant**
1446 **decisions during locomotion.**

1447 **a**, Representative image of virus-expressing M2 axons in subregions of the anterior AC. Scale
1448 bar, 500 μm. Inset, an example injection site in M2. Scale bar, 1 mm.

1449 **b**, Percentages of labeled neurons (black) and M2 axon intensity (green) in anterior AC
1450 subregions. Solid line, AC_{PPC} neurons; dotted line, AC_{STR} neurons.

1451 **c**, Schematic illustration of *in vivo* calcium imaging of projection-specific AC neurons
1452 combined with optogenetic activation of M2 axons in the AC using the nVoke system.

1453 **d**, Response amplitudes of AC_{PPC} neurons (left) and AC_{STR} neurons (right) to 10kHz or 5kHz
1454 pure tones. Yellow, optogenetic activation of M2 axons; Off, LED-off; On, LED-on.

1455 **e**, Schematic illustration of *in vivo* calcium imaging of $M2_{AC}$ neurons.

1456 **f**, Calcium activity of $M2_{AC}$ neurons during incongruent trials. Black, visual-dominant trials;
1457 gray, auditory-dominant trials; solid, $A_{NG}V_G$ trials; dotted, A_GV_{NG} trials. Magenta, stimulus
1458 onset (solid) and offset (dashed).

1459 **g**, Peri-stimulus mean activity (-1 to 1 s from onset) of $M2_{AC}$ neurons across incongruent trials.

1460 **h**, Distribution of Pearson correlation coefficients between calcium activity and locomotion
1461 onset across individual $M2_{AC}$ neurons. Magenta, zero line.

1462 **i**, Top, mean activity of $M2_{AC}$ neurons after locomotion onset. Magenta, locomotion onset;
1463 lighter gray shade, early locomotion period (0 ~ 1.5 s after onset); darker gray shade, late
1464 locomotion period (> 3 s after onset). Bottom, mean activity of $M2_{AC}$ neurons during early and
1465 late locomotion periods.

1466 **j**, Schematic illustration of optogenetic inhibition of M2 axons in the AC in task-performing
1467 mice during movement.

1468 **k**, Changes in d′ (left), hit rates (middle), and FA rates (right) following optogenetic inhibition
1469 of M2 axon terminals in the AC.

Data are presented as means ± SEM. Thin lines represent individual data. For box plots, central lines indicate medians; boxes represent the 25th-75th percentiles; whiskers show maximum/minimum values excluding outliers. Source data are available in Source Data File. Sample numbers and statistical information are listed in Supplementary Data 1. NS, not significant; #$P < 0.1$, *$P < 0.05$, **$P < 0.01$, ***$P < 0.001$, ****$P < 0.0001$.

1475 **Fig. 9 | Schematic illustration of sensory dominance switching during locomotion.**
1476 Left, auditory dominance in stationary mice, driven by auditory-to-visual suppression in the
1477 PPC. Right, M2-mediated gating of the AC-to-PPC circuit induces visual dominance during
1478 locomotion.

Figure 1

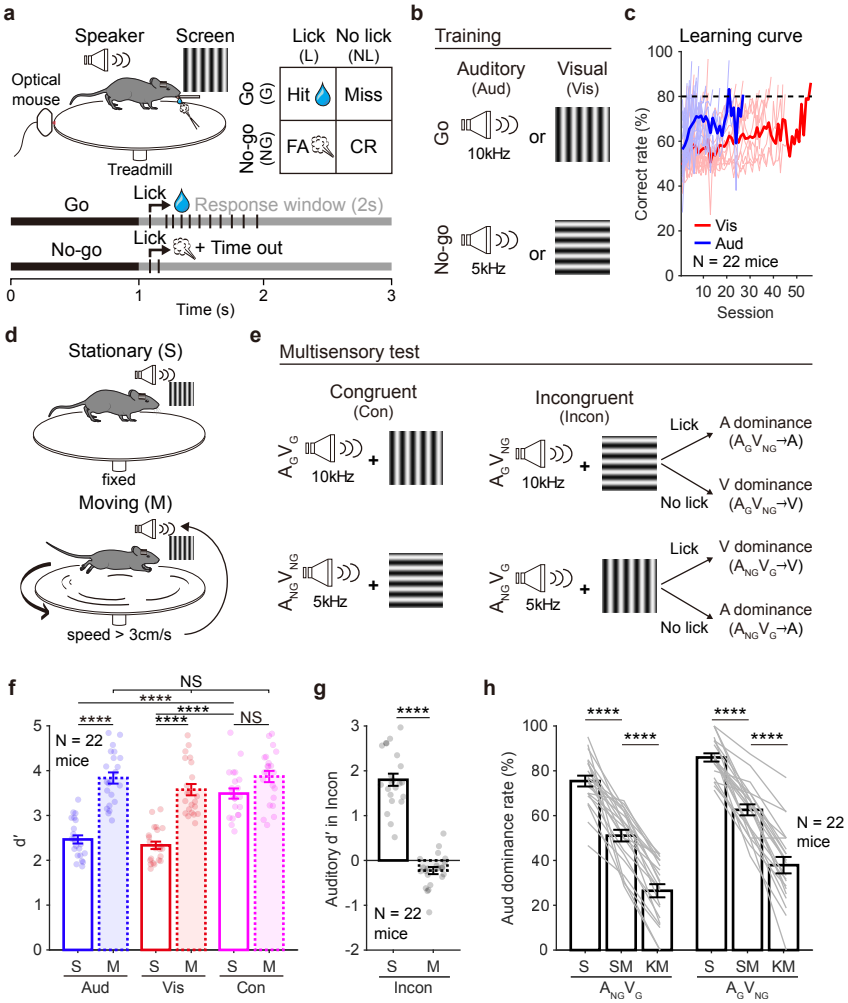
a
Speaker
Screen
Optical mouse
Treadmill
Lick (L)
No lick (NL)
Go (G)
No-go (NG)
Hit
Miss
FA
CR
Go
Lick
Response window (2s)
No-go
Lick
+ Time out
Time (s)
b
Training
Auditory (Aud)
Visual (Vis)
Go
10kHz
or
No-go
5kHz
c
Learning curve
Correct rate (%)
Vis
Aud
N = 22 mice
Session
d
Stationary (S)
fixed
Moving (M)
speed > 3cm/s
e
Multisensory test
Congruent (Con)
Incongruent (Incon)
10kHz
5kHz
Lick
No lick
A dominance
V dominance
f
NS
N = 22 mice
d'
S
M
Aud
Vis
Con
g
Auditory d' in Incon
N = 22 mice
Incon
h
Aud dominance rate (%)
N = 22 mice
S
SM
KM

Figure 2

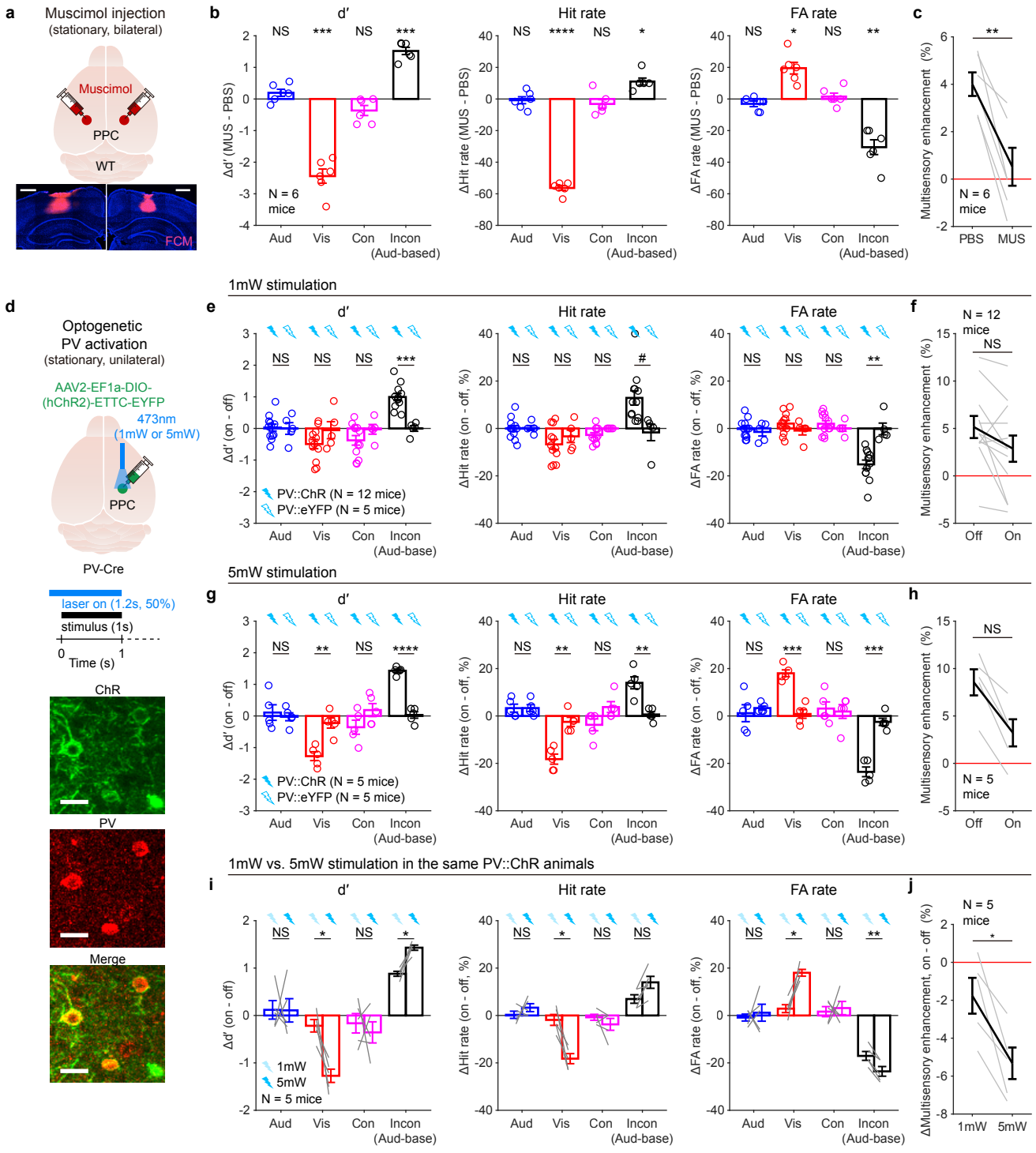
a
Muscimol injection
(stationary, bilateral)
Muscimol
PPC
WT
FCM
b
d'
Hit rate
FA rate
Δd' (MUS - PBS)
ΔHit rate (MUS - PBS)
ΔFA rate (MUS - PBS)
N = 6 mice
Aud
Vis
Con
Incon
(Aud-based)
c
Multisensory enhancement (%)
N = 6 mice
PBS
MUS
1mW stimulation
d
Optogenetic
PV activation
(stationary, unilateral)
AAV2-EF1a-DIO-
(hChR2)-ETTC-EYFP
473nm
(1mW or 5mW)
PPC
PV-Cre
laser on (1.2s, 50%)
stimulus (1s)
Time (s)
ChR
PV
Merge
e
Δd' (on - off)
ΔHit rate (on - off, %)
ΔFA rate (on - off, %)
PV::ChR (N = 12 mice)
PV::eYFP (N = 5 mice)
(Aud-base)
f
N = 12 mice
Off
On
5mW stimulation
g
PV::ChR (N = 5 mice)
PV::eYFP (N = 5 mice)
h
N = 5 mice
1mW vs. 5mW stimulation in the same PV::ChR animals
i
1mW
5mW
N = 5 mice
j
N = 5 mice
ΔMultisensory enhancement, on - off (%)
1mW
5mW

Figure 3

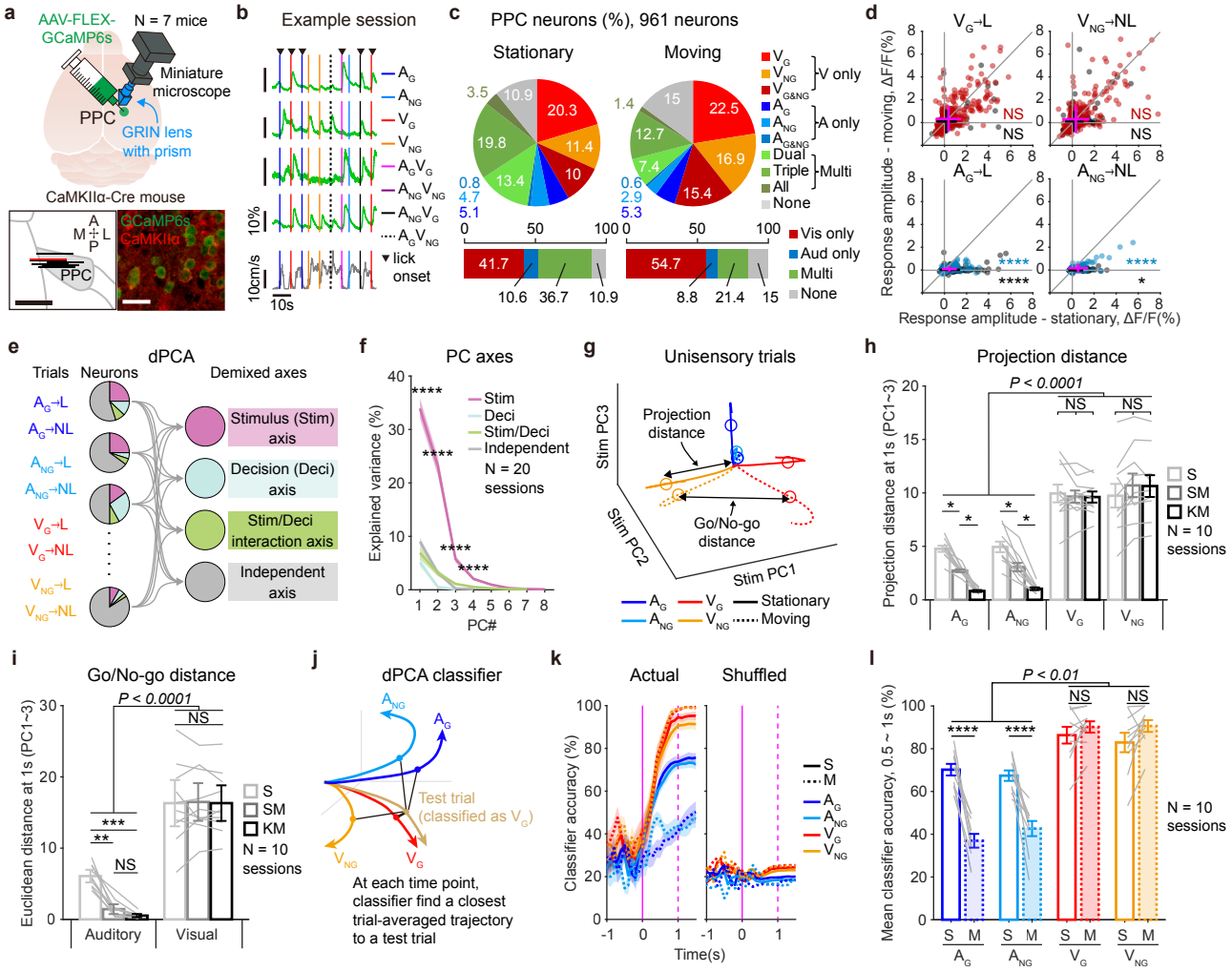
a
AAV-FLEX-GCaMP6s
N = 7 mice
Miniature microscope
PPC
GRIN lens with prism
CaMKIIα-Cre mouse
GCaMP6s
CaMKIIα
b
Example session
lick onset
10%
10cm/s
10s
c
PPC neurons (%), 961 neurons
Stationary
Moving
V only
A only
Multi
Vis only
Aud only
Multi
None
d
Response amplitude - moving, ΔF/F(%)
Response amplitude - stationary, ΔF/F(%)
NS
e
dPCA
Trials
Neurons
Demixed axes
Stimulus (Stim) axis
Decision (Deci) axis
Stim/Deci interaction axis
Independent axis
f
PC axes
Explained variance (%)
PC#
Stim
Deci
Stim/Deci
Independent
N = 20 sessions
g
Unisensory trials
Projection distance
Go/No-go distance
Stim PC1
Stim PC2
Stim PC3
Stationary
Moving
h
Projection distance
Projection distance at 1s (PC1~3)
P < 0.0001
NS
S
SM
KM
N = 10 sessions
i
Go/No-go distance
Euclidean distance at 1s (PC1~3)
P < 0.0001
Auditory
Visual
j
dPCA classifier
Test trial (classified as V_G)
At each time point, classifier find a closest trial-averaged trajectory to a test trial
k
Actual
Shuffled
Classifier accuracy (%)
Time(s)
l
Mean classifier accuracy, 0.5 ~ 1s (%)
P < 0.01
N = 10 sessions

Figure 4

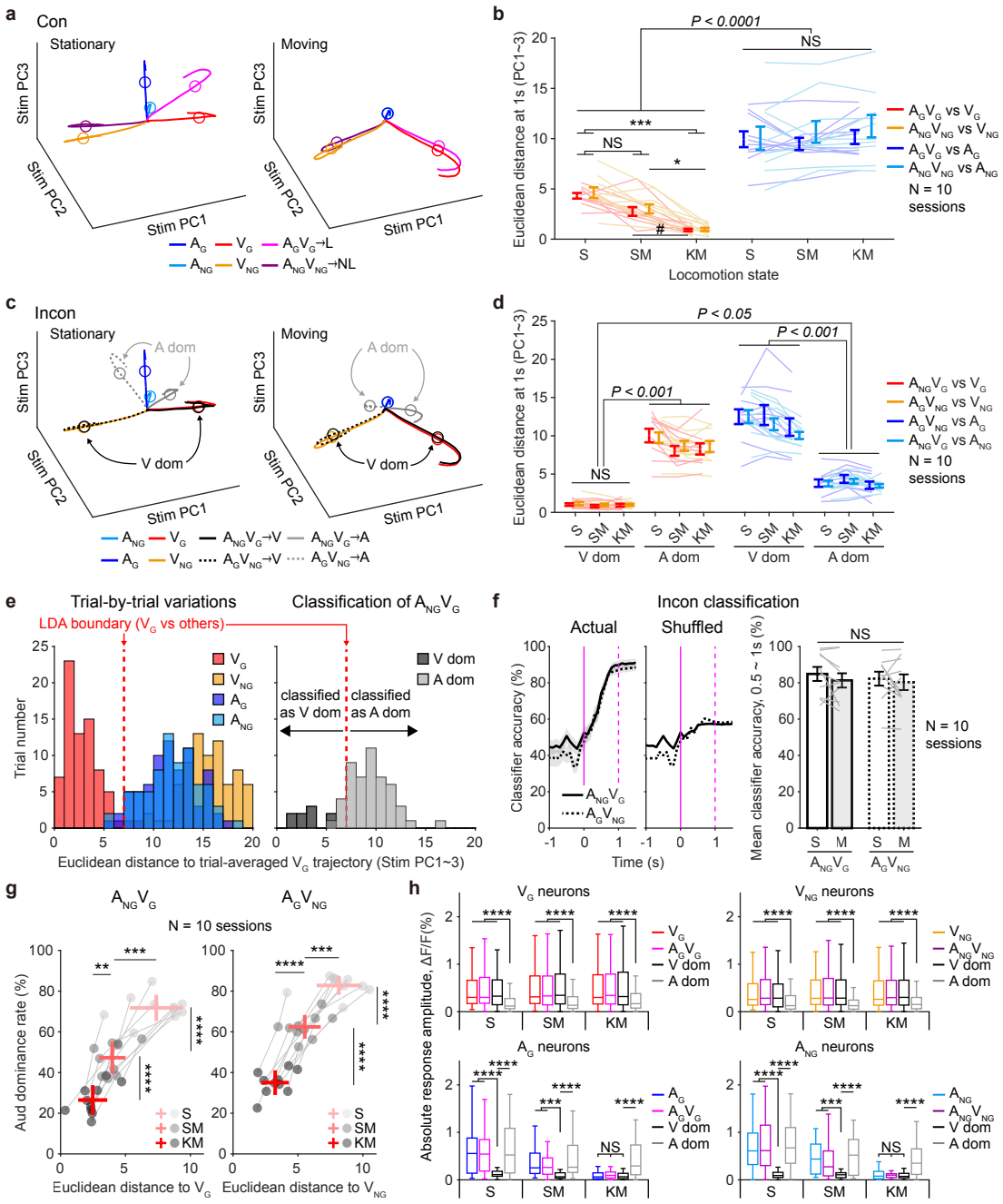
a
Con
Stationary
Moving
Stim PC3
Stim PC2
Stim PC1
A_G V_G A_GV_G→L
A_{NG} V_{NG} $A_{NG}V_{NG}$→NL
b
P < 0.0001
NS
***
NS
*
#
Euclidean distance at 1s (PC1~3)
Locomotion state
S SM KM S SM KM
A_GV_G vs V_G
$A_{NG}V_{NG}$ vs V_{NG}
A_GV_G vs A_G
$A_{NG}V_{NG}$ vs A_{NG}
N = 10 sessions
c
Incon
Stationary
Moving
A dom
V dom
A_{NG} V_G $A_{NG}V_G$→V $A_{NG}V_G$→A
A_G V_{NG} A_GV_{NG}→V A_GV_{NG}→A
d
P < 0.05
P < 0.001
P < 0.001
NS
$A_{NG}V_G$ vs V_G
A_GV_{NG} vs V_{NG}
A_GV_{NG} vs A_G
$A_{NG}V_G$ vs A_{NG}
N = 10 sessions
V dom A dom V dom A dom
e
Trial-by-trial variations
Classification of $A_{NG}V_G$
LDA boundary (V_G vs others)
Trial number
V_G V_{NG} A_G A_{NG}
V dom A dom
classified as V dom
classified as A dom
Euclidean distance to trial-averaged V_G trajectory (Stim PC1~3)
f
Incon classification
Actual
Shuffled
Classifier accuracy (%)
$A_{NG}V_G$ A_GV_{NG}
Time (s)
Mean classifier accuracy, 0.5 ~ 1s (%)
NS
N = 10 sessions
S M S M
$A_{NG}V_G$ A_GV_{NG}
g
$A_{NG}V_G$
A_GV_{NG}
N = 10 sessions
Aud dominance rate (%)
S SM KM
Euclidean distance to V_G
Euclidean distance to V_{NG}
h
V_G neurons
V_{NG} neurons
A_G neurons
A_{NG} neurons
Absolute response amplitude, ΔF/F (%)
V_G A_GV_G V dom A dom
V_{NG} $A_{NG}V_{NG}$ V dom A dom
A_G A_GV_G V dom A dom
A_{NG} $A_{NG}V_{NG}$ V dom A dom
S SM KM

Figure 5

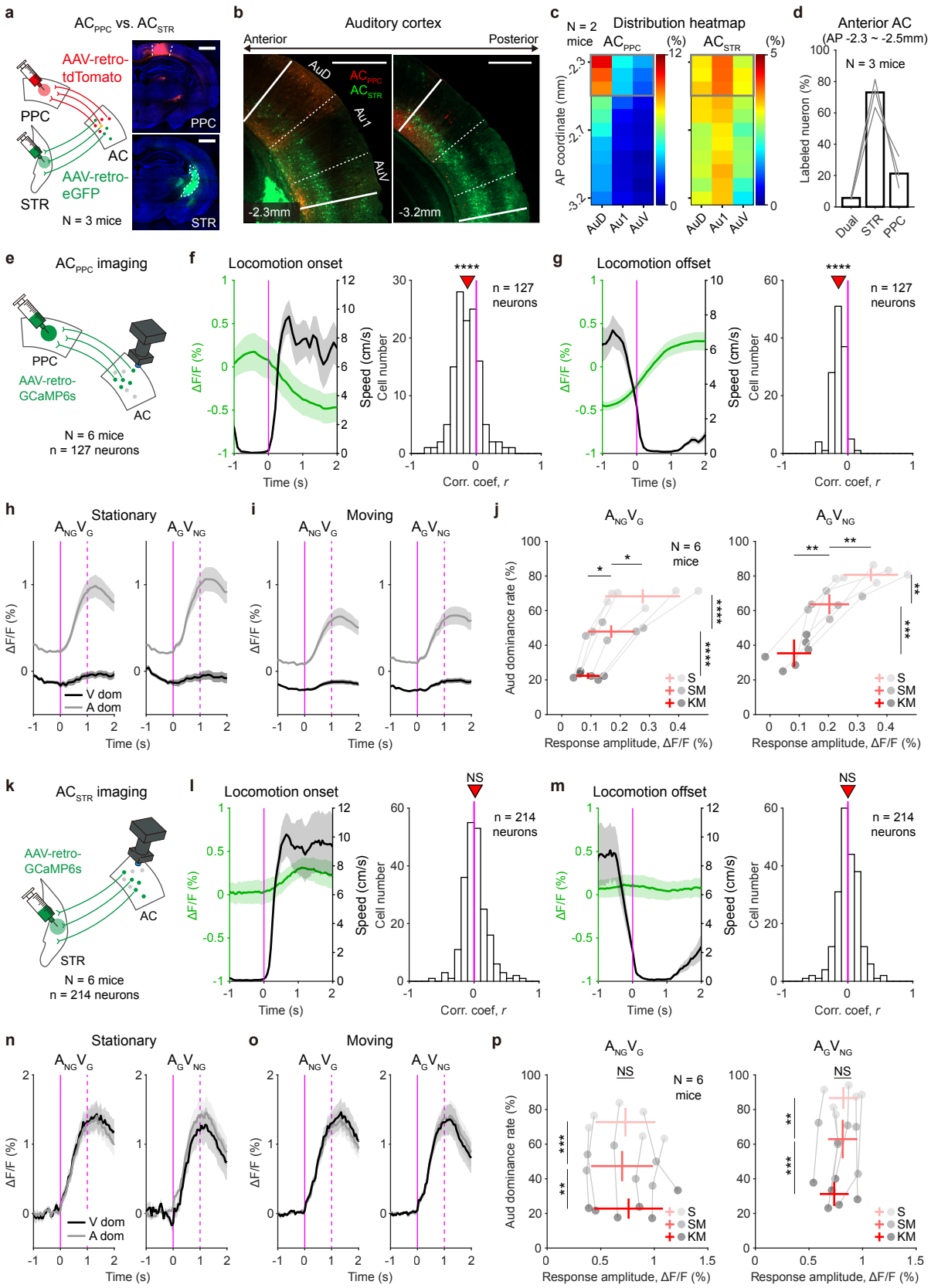
a
AC_PPC vs. AC_STR
AAV-retro-tdTomato
PPC
AC
AAV-retro-eGFP
STR
N = 3 mice
b
Auditory cortex
Anterior
Posterior
AuD
Au1
AuV
-2.3mm
-3.2mm
c
N = 2 mice
Distribution heatmap
AP coordinate (mm)
d
Anterior AC
(AP -2.3 ~ -2.5mm)
N = 3 mice
Labeled nueron (%)
Dual
e
AC_PPC imaging
AAV-retro-GCaMP6s
N = 6 mice
n = 127 neurons
f
Locomotion onset
ΔF/F (%)
Speed (cm/s)
Cell number
Time (s)
Corr. coef, r
n = 127 neurons
g
Locomotion offset
h
Stationary
V dom
A dom
i
Moving
j
Aud dominance rate (%)
Response amplitude, ΔF/F (%)
S
SM
KM
k
AC_STR imaging
l
n = 214 neurons
m
NS
n
o
p

Figure 6

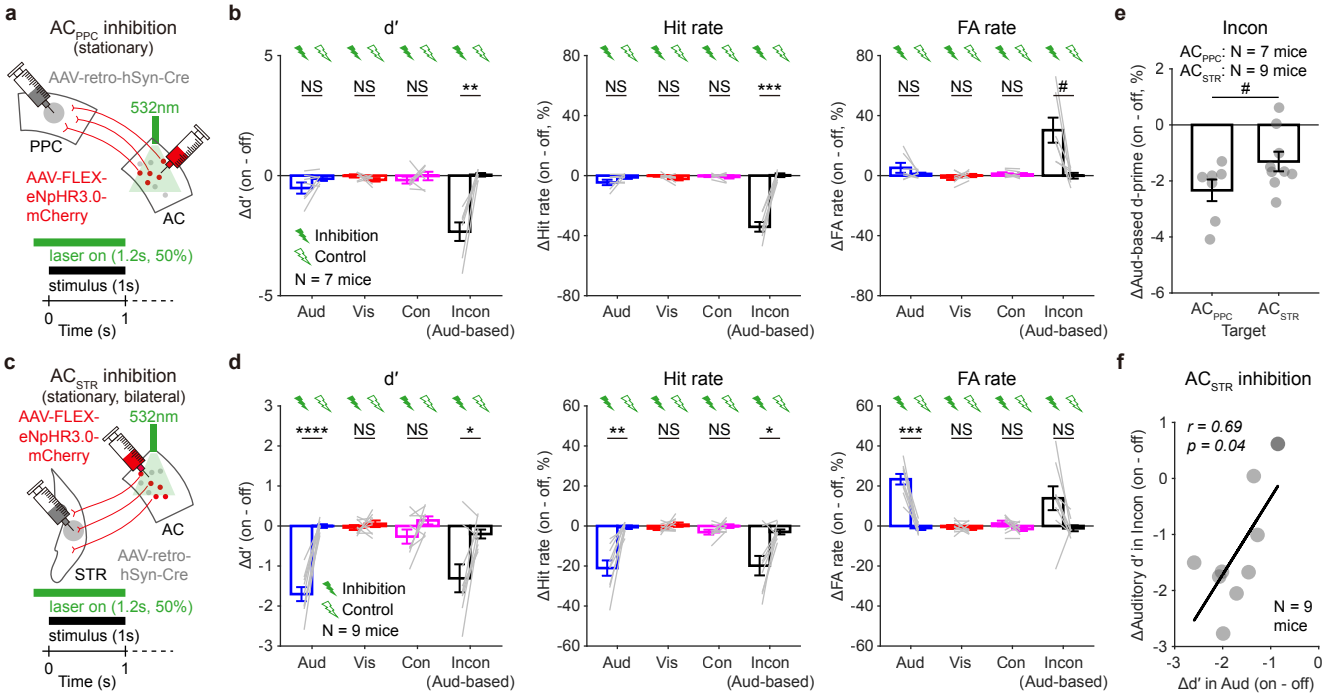
a
AC$_{PPC}$ inhibition
(stationary)
AAV-retro-hSyn-Cre
532nm
PPC
AAV-FLEX-
eNpHR3.0-
mCherry
AC
laser on (1.2s, 50%)
stimulus (1s)
0
1
Time (s)
b
d′
Δd′ (on - off)
NS NS NS **
Inhibition
Control
N = 7 mice
Aud Vis Con Incon
(Aud-based)
Hit rate
ΔHit rate (on - off, %)
NS NS NS ***
FA rate
ΔFA rate (on - off, %)
NS NS NS #
e
Incon
AC$_{PPC}$: N = 7 mice
AC$_{STR}$: N = 9 mice
#
ΔAud-based d-prime (on - off, %)
AC$_{PPC}$ AC$_{STR}$
Target
c
AC$_{STR}$ inhibition
(stationary, bilateral)
AAV-FLEX-
eNpHR3.0-
mCherry
532nm
AC
STR
AAV-retro-
hSyn-Cre
laser on (1.2s, 50%)
stimulus (1s)
0
1
Time (s)
d
d′
Δd′ (on - off)
**** NS NS *
Inhibition
Control
N = 9 mice
Aud Vis Con Incon
(Aud-based)
Hit rate
ΔHit rate (on - off, %)
** NS NS *
FA rate
ΔFA rate (on - off, %)
*** NS NS NS
f
AC$_{STR}$ inhibition
r = 0.69
p = 0.04
N = 9
mice
ΔAuditory d′ in Incon (on - off)
Δd′ in Aud (on - off)

Figure 7

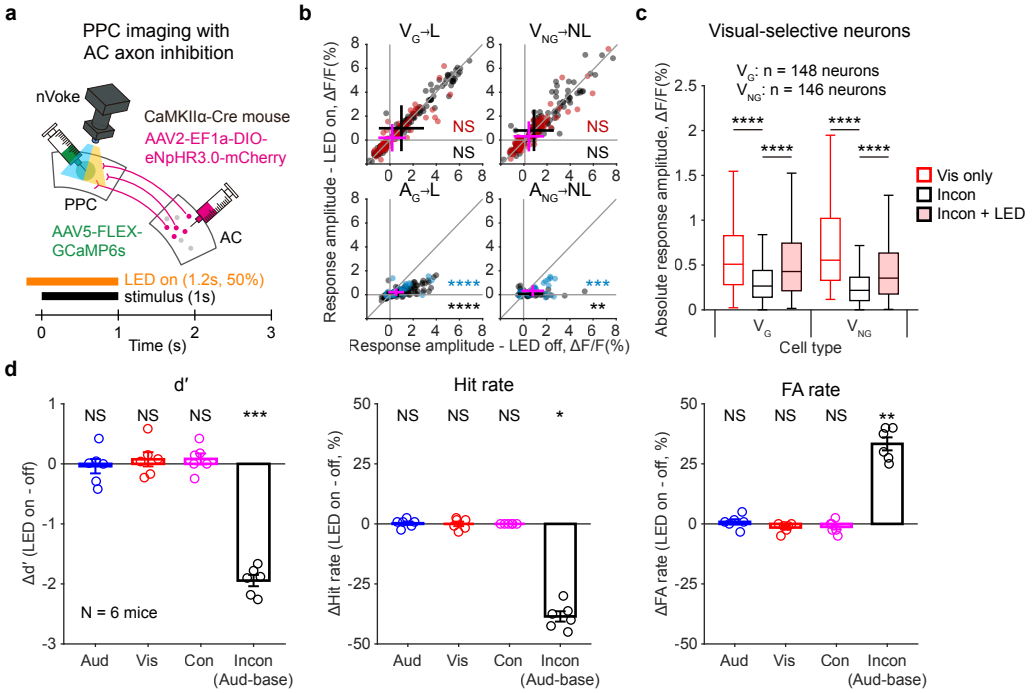
a
PPC imaging with
AC axon inhibition
nVoke
CaMKIIα-Cre mouse
AAV2-EF1a-DIO-
eNpHR3.0-mCherry
PPC
AC
AAV5-FLEX-
GCaMP6s
LED on (1.2s, 50%)
stimulus (1s)
Time (s)
b
Response amplitude - LED on, ΔF/F(%)
Response amplitude - LED off, ΔF/F(%)
NS
****
***
**
c
Visual-selective neurons
Absolute response amplitude, ΔF/F(%)
Cell type
Vis only
Incon
Incon + LED
d
d′
Δd′ (LED on - off)
N = 6 mice
Hit rate
ΔHit rate (LED on - off, %)
FA rate
ΔFA rate (LED on - off, %)
Aud
Vis
Con
Incon
(Aud-base)

Figure 8

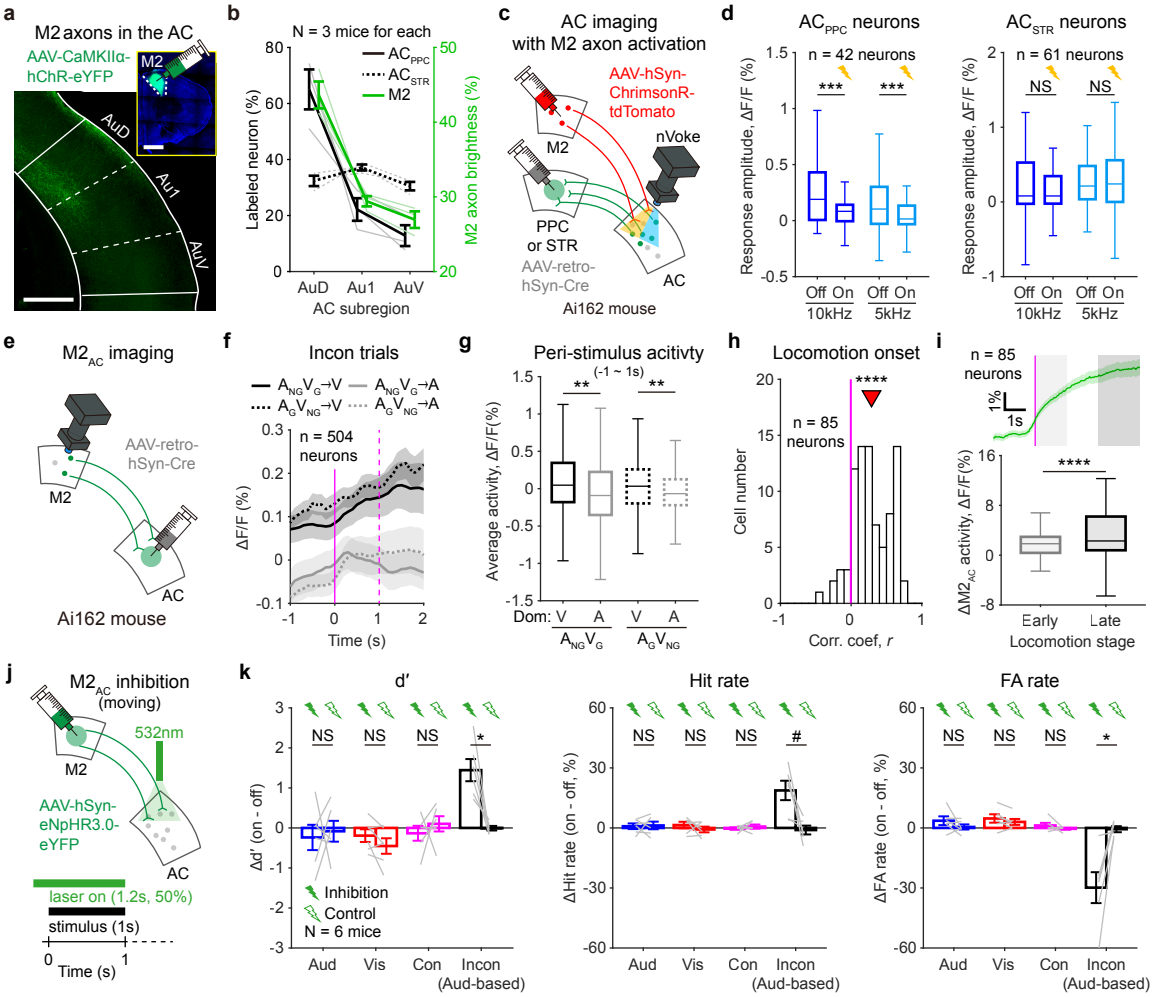
a
M2 axons in the AC
AAV-CaMKIIα-hChR-eYFP
M2
AuD
Au1
AuV
b
N = 3 mice for each
Labeled neuron (%)
M2 axon brightness (%)
AC subregion
c
AC imaging with M2 axon activation
AAV-hSyn-ChrimsonR-tdTomato
nVoke
M2
PPC or STR
AAV-retro-hSyn-Cre
AC
Ai162 mouse
d
AC_PPC neurons
AC_STR neurons
n = 42 neurons
n = 61 neurons
Response amplitude, ΔF/F (%)
Off On Off On
10kHz 5kHz
e
M2_AC imaging
AAV-retro-hSyn-Cre
M2
AC
Ai162 mouse
f
Incon trials
n = 504 neurons
ΔF/F (%)
Time (s)
g
Peri-stimulus acitivty
(-1 ~ 1s)
Average activity, ΔF/F(%)
Dom: V A V A
h
Locomotion onset
n = 85 neurons
Cell number
Corr. coef, r
i
n = 85 neurons
1%
1s
ΔM2_AC activity, ΔF/F(%)
Early Late
Locomotion stage
j
M2_AC inhibition (moving)
532nm
M2
AAV-hSyn-eNpHR3.0-eYFP
AC
laser on (1.2s, 50%)
stimulus (1s)
Time (s)
k
d'
Hit rate
FA rate
Δd' (on - off)
ΔHit rate (on - off, %)
ΔFA rate (on - off, %)
Inhibition
Control
N = 6 mice
Aud Vis Con Incon
(Aud-based)

Figure 9

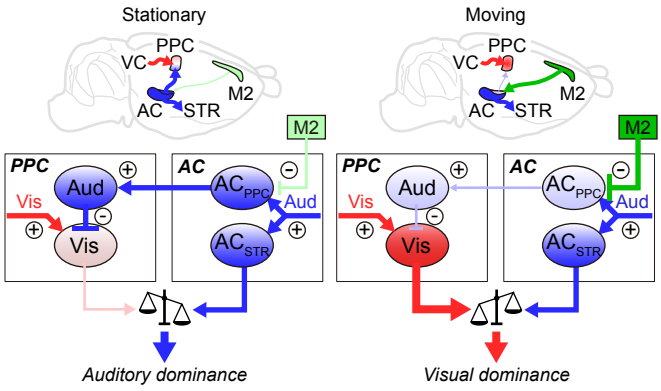
Stationary
PPC
VC
M2
AC
STR
M2
PPC
Aud
Vis
Vis
AC
AC_PPC
Aud
AC_STR
Auditory dominance
Moving
PPC
VC
M2
AC
STR
M2
PPC
Aud
Vis
Vis
AC
AC_PPC
Aud
AC_STR
Visual dominance